CERN/DRDC/90–31
DRDC/P5
13th August, 1990

R&D PROPOSAL

LIQUID ARGON CALORIMETRY WITH LHC–PERFORMANCE SPECIFICATIONS

B. Aubert, B. Beaugiraud, F. Cavanna, J. Colas, A. Daba, M. Maire, J.P. Vialle
LAPP, Annecy, France

H.A. Gordon, V. Polychronakos, V. Radeka, D. Rahm, S. Rescia, I. Stumer
Brookhaven National Laboratory, Upton, USA

C.W. Fabjan[2], O. Gildemeister, P. Jenni, M. Lefebvre, M. Nessi,
F. Nessi-Tedaldi, M. Pepe, G. Polesello, G.R. Stevenson, W.J. Willis
CERN, Geneva, Switzerland

C. Battistoni*, C. Birattari, D. Camin, D. Cavalli, G. Costa, A. Ferrari,
F. Gianotti, L. Mandelli, M. Mazzanti, L. Perini
Dipartimento di Fisica dell'Università e Sezione INFN, Milano, Italy

E. Augé, J.C. Chollet, C. de la Taille, L. Fayard, D. Fournier[1], J.M. Gaillard,
G. Guilhem, A. Hrisoho, L. Iconomidou-Fayard, B. Merkel, J.M. Noppe,
G. Parrour, P. Pétroff, J.P. Repellin, A. Schaffer, N. Seguin
LAL, Orsay, France

C. Fuglesang
Manne Siegbahn Institute, Stockholm, Sweden

1) Spokesperson
2) Contactperson
* Present address: L.N.F., Frascati, Italy

Abstract

A broad R&D programme is proposed to study and improve the performance of LAr calorimetry required to meet LHC specifications. Novel readout structures with high granularity and very short cable connections will permit to achieve a high readout speed and minimal dead space. Design, simulations and substantial prototype studies are proposed in order to investigate physics and engineering aspects of a LAr calorimeter for LHC. It is planned to develop fast and radiation resistant LAr electronics, both based on Si JFET and GaAs technologies.

1. INTRODUCTION

There is widespread consensus that good electromagnetic and hadronic calorimetry will have a central place in an LHC detector, independent of the particular physics topics emphasized and for most of the overall experimental strategies followed. Several reasons contribute to the importance of this measurement technique in the context of LHC experimentation:

- the calorimeter will be the major tool to measure energies and directions for electrons (and photons), for quark and gluon jets and for neutrinos and other weakly interacting particles. These measurements are expected to signal most convincingly the new physics phenomena;

- the calorimetric energy measurements will be available relatively fast, even on the time scale of LHC collisions rates. They will permit a powerful discrimination, already at the trigger level, between rare events of interest and the 'noise' of ordinary hadronic collisions (minimum bias events) occurring at a ferocious rate at high luminosities;

- it will reliably separate high energy final state particles from the large flux of particles expected from several minimum bias events overlapping in the same or nearby beam crossings (pile–up) at high luminosities.

The physics goals and the collider environment will be very demanding on many performance aspects of an LHC calorimeter [1]. None of the available techniques, whether matured during the last decade or even those as yet untested with a significant prototype, can already be considered as fully satisfactory solutions. Only dedicated work to explore and improve the weaknesses of a given technique may ultimately lead to an instrument of high enough quality such that the discovery potential of the LHC is fully exploited.

Such an R&D programme should include several selected techniques: calorimetry based on the Liquid Argon (LAr) ion chamber technique is the subject of this Proposal. Its potential for experimentation at future high luminosity hadron colliders has been discussed in Ref. [2]. Typical performance parameters achievable with LAr calorimetry are listed in Table 1, which we consider very attractive in view of the LHC physics goals at high luminosities. We have selected the LAr technique in particular also for the following reasons:

- the granularity of the electromagnetic (e.m.) calorimeter imposes the most stringent mechanical and electronic constraints. Of all techniques used in experiments to date, the LAr methods appear to us, in balance, to satisfy this requirement best;
- very good e.m. energy resolution with negligible constant term can be achieved as well as adequate jet resolution with excellent response uniformity;
- it is arguably a very stable, uniform and robust calorimeter readout technique. These are important virtues when experimenting in one of the most hostile environments ever encountered;
- the LAr device is very radiation resistant. Progress has been made in strengthening the one weak element – the preamplifier, as will be discussed in Chapters 4 and 6.

There are, however, several points requiring attention and clarification before a LAr calorimeter can be proposed for LHC. They are briefly outlined here. The proposed R&D programme specifically addresses these points.

1.1 Temporal Response

First, we analyse the temporal response of ion chamber calorimeters, which becomes a major concern for LHC operation. We briefly indicate the temporal performance achievable, state the performance obtained to date and describe our thinking on further improvements. This work is motivated by our intention to operate the detector at luminosities of up to $L = 2 \times 10^{34}\ cm^2\ s^{-1}$.

When evaluating the rate capability of such detectors it is useful to distinguish between the occupation time (i.e. the duration of the physical signature produced by the passage of a particle) and the response time of the signal processing electronics controlled by signal 'shaping' and which ultimately determines the rate capability of the detector. For high–rate operation it is advantageous to chose 'equal–area' bipolar shaping which ensures that the superposition or 'pile–up' of several events within the sensitive time of the detector *does not, on average,* produce a net shift in the measurement of a large signal. Pile–up will, however, contribute as noise, σ (pile–up), to the overall energy resolution of the detector. The result of several quantitative studies on σ (pile–up) as a function of interaction rate n and the pulse shaping or the peaking time t_p of the signal have been carried out [3] and are summarized in Fig. 1 (see the figure caption for further explanations). As an example, at a luminosity of $L = 20\ nb^{-1}s^{-1}$ ($L = 2 \times 10^{34}\ cm^{-2}\ s^{-1}$, $n \approx 20$ collisions per bunch crossing) and a peaking time $t_p = 50$ ns, one expects a level of σ (pile–up) $\approx$ 0.7 GeV for a solid angle of $\Delta\phi \cdot \Delta\eta = 0.06 \times 0.06$, typical for the size of an electromagnetic shower, increasing to $\sigma \sim 10$ GeV for a typical jet–cone with half angle $\alpha = 30^o$.

In principle, this pile–up noise could be reduced further by increasingly faster shaping. This has to be balanced, however, by the loss in the effective charge Q sampled and the increase in the electronic noise N of the preamplifier. As an example, the observed noise level of the HELIOS calorimeter [4] as a function of peaking time t_p is also indicated in Fig. 1. The graph also indicates the virtue of faster liquids, which may deliver more charge into the preamplifier for a given peaking time t_p. One should note, however, that such a performance can only be achieved if the charge collected can be transferred from the detector electrodes to the preamplifier on a time scale comparable to or shorter than the peaking time [5]. This is technically possible, provided the total cable length remains short, typically less than 1 m. For LHC type devices therefore, amplifiers will have to be embedded inside the calorimeter and will have to be operated at temperatures in the vicinity of ~ 100 K. The latter condition has already been realized in the HELIOS calorimeter [4] although not in a way which can easily be adapted to the geometry of collider detectors.

We are confronted therefore with the problem of a detector construction that combines a highly granular tower readout, very short cable connections with essentially no dead space. We propose a novel detector readout geometry to solve these difficulties. We have prepared a small calorimeter and have tested this concept in July 1990. A description of this prototype, its construction, signal readout and simulated performance are presented in Chapter 2.

The other desirable ingredient – faster drift velocities – by using dopants such as CH_4 is the subject of another R&D proposal, which aims at a systematic study of the effects of dopants on liquid argon properties and it is not further developed here.

An integral aspect of a fast ion–chamber calorimeter is the signal processing. We wish to concentrate, in this proposal, on the very critical analog front–end, as described in Chapters 2 and 4. We are presently pursuing the development of Si JFET front–ends and in parallel novel GaAs preamplifiers. The latter hold the promise of lower noise, lower power consumption and higher radiation tolerance.

1.2 Compensation in LAr Calorimeters

Adequate compensation is required in high–performance calorimeters. In the past it has been demonstrated that precise compensation is achievable in U/Scintillators and Pb/Scintillator calorimeters; approximate compensation has been also measured in U/LAr calorimeters and one result [4] is shown in Fig. 2.

While this level of compensation in a U/LAr calorimeter is probably adequate, we wish to pursue compensation studies in a Pb/LAr calorimeter with the aim to avoid the complication of handling uranium. In our view there are two independent handles available to tune 'e/h'. The first aims to suppress the electron response by using a sandwich of two materials with very different critical energies ε [6]. The second 'knob' to tune 'e/h' would be to enhance the hadronic response; this may be possible if one could reduce the effective saturation properties of LAr as a function of the ionization density. A way towards this goal may be the addition of photosensitive dopants, which convert the non–saturating scintillation light of LAr into collectable charges (see the 'Dopant'–proposal previously mentioned).

In the present proposal we wish to address the 'electron suppression' scheme through detailed hadronic shower Monte Carlos, as outlined in Chapter 5. Furthermore, we plan, in a complementary study, to evaluate the effect of non–perfect compensation on the energy resolution and linearity of jets.

1.3 Hermeticity and Uniformity of Response

Another frequently voiced concern about LAr calorimeters is the possible interference of cryostat walls with hermetic coverage. Considerable design work is needed to obtain quantitative results, as demonstrated by a recent engineering study [7]. In addition to cryostat walls, non–instrumented space occupied by cables and support structures is potentially even more deleterious as it may affect the uniformity in energy response. We wish to carry out a comprehensive design study to implement our novel readout structure in a detector with large rapidity coverage and with good and uniform response, while keeping non–instrumented space and particle leakage through cryostat walls acceptably low. This programme on the design of possible calorimeter structures is described in Chapter 3.

1.4 Principle Objectives of the Proposal

We summarize the principle directions we propose to pursue. Our aim is to study and to improve certain performance aspects of a LAr calorimeter such that the performance requirements imposed by the LHC discovery potential can be met.

Specifically, we wish to carry out:

- the testing and evaluation of a novel readout structure, which allows the high granularity needed for the e.m. calorimeter, while permitting very short cable connections to achieve a high readout speed and minimal dead space;
- a comprehensive design study, covering the physics and engineering aspects of a LAr calorimeter with large rapidity acceptance, which could be part of an LHC experiment;

- a programme to develop fast preamplifiers, both based on Si JFET and new GaAs technology. The radiation hardness of these preamplifiers will also be evaluated;
- an extensive simulation programme to evaluate the
  - level of compensation in Pb/LAr calorimeters,
  - the impact of calorimeter parameters (e.g. granularity, segmentation) on the systems performance;
- an evaluation of the radiation resistance of calorimeter components.

2. A NOVEL CALORIMETER CONCEPT: THE ACCORDION

2.1 Motivation

In the conventional approach of liquid argon calorimetry, converter and readout electrodes are planar parallel plates. Basic detector elements, connected to one preamplifier channel, are then formed by ganging together, over a certain depth, corresponding strips or pads (Fig.3a). When the required granularity is high, ganging by tie rods crossing the calorimeter planes becomes unpractical. The usual solution consists of bringing signals in each plane to the edges of a module, where the connections are made.

The highest granularity reached in this way is that of the HELIOS calorimeter where pads of 2 cm by 2 cm cover an area of about 0.5 m^2 [4]. This scheme implies dead space around modules, additional capacity from the (shielded) lines to the module edges, and additional inductance from those same lines. Capacity and inductance of a detector element, together with the preamplifier characteristics, determine the noise and speed of response, and therefore the calorimeter performances [5]. This construction does not lend itself to a signal speed adequate for high–luminosity LHC operation.

The adverse effects of this connection system can be solved by a novel scheme which we propose. The converter plates and readout electrodes are no longer planar, but instead have an accordion shape (Fig. 3b). In this case the connection of successive pads to form a tower element is automatic. With a preamplifier mounted on the front and back face of the calorimeter, directly on each detector element, the most favourable situation for reduced noise, maximum speed and low cross–talk has been achieved. The accordion shape is also well suited for minimum dead space between modules (see section 3). The question of resolution and uniformity of response in energy and position deserves however detailed study.

In the following sections we describe the mechanics and electronics of the prototype of an e.m. section that we have built for this purpose. The design of this calorimeter has been based on detailed shower simulation, which we also briefly describe.

2.2 The prototype calorimeter and its mechanical structure

A module of transverse section 40 cm by 50 cm, and 25 radiation lengths depth has been built, which allows nearly complete electron shower containment at SPS energies and uniformity studies. The converter plates are made of 1.8 mm lead (purity 99.9%) foils clad in 0.1 mm stainless steel. The readout electrodes are made of polyimide 'Kapton' copper–clad boards. Both the converter and readout plates have an accordion shape with a pitch of 40.1 mm and an angle of inclination of 45^{o} with respect to the nominal direction of incidence. The argon gap on either side of the Kapton foil is 1.9 mm. The separation between the electrodes is ensured by inserting bands of 'Hexcell' between the flat parts of the electrodes. Towers are formed by chemically etching strips 25 mm wide on the copper cladding (Fig. 4). In the present design, these strips are cut longitudinally in two equal sections, thus giving two samplings of 12.5 radiation lengths each.

In order to reach good uniformity in energy response, the mechanics of this calorimeter has to be built with rather tight tolerances. For this purpose, a fabrication procedure for the lead–stainless steel (SS) sandwiches has been developed at CERN in collaboration with Stesalit AG (Zullwil, Switzerland). It uses "prepreg" layers which polymerise under pressure at around 120^{o}. They can be manipulated with their protection film for a few hours at room temperature. In a first step the prepregs are put in contact with the SS while their other side still has the protection film. The lead is then sandwiched in between two such layers, and the package formed in this way is bent into the desired accordion shape using a tool developed at CERN for this purpose (Fig. 5). In a second step, the remaining protection films are removed, and the SS plates are again put in contact with the lead. This sandwich has the final structure, but the glue is not yet polymerised. It is stored for a few days, under argon atmosphere, at -18^{o}. In the last step the sandwiches are transported to Stesalit where the final gluing (2 hours at 120^{o} at 5 Kg/cm^2) is carried out using a specially constructed mould.

The readout electrodes, as shown in Fig. 6, consist of 4 conductive layers separated by 25 μm polyimide (and glue). The outside layers, at high voltage, produce, together with the lead/SS plates at ground, the electric field in which the electrons (resulting from ionisation of the liquid argon) will drift. The signal produced in this way is coupled through the resistive coating to the strips of the central layers, which are DC–coupled to the preamplifiers. The distributed blocking capacity formed in this way is about 30 times larger than the capacity to ground. In order to protect the preamplifiers from accidental sparking, the HV external layers are made of a resistive coating. The readout electrodes are produced flat, with the now standard fabrication techniques for flexible circuits. They are then bent to the desired accordion shape using the same tooling used for the lead/SS sandwich. Since the resistive layer is rather fragile, the copper cladding is preserved for ± 5 mm centred at the place of each bend.

The thickness of the readout electrode is 400 μm. The bend radii are the same as for the lead/SS sandwich (3 mm), as well as the accordion pitch (40.1 mm).

A condition for good uniformity of response is that the average ratio of liquid argon to other materials (mainly lead) varies as little as possible as a function of the impact point on the calorimeter. Due to the chosen geometry, this is particularly critical at normal incidence where "corners" align themselves with the beam particle. To study these effects, a computer code has been written to analytically compute the thickness of liquid argon as a function of the impact distance to a reference point on an accordion cell. Fixing the material thicknesses and accordion pitch, one can optimise the liquid argon gap to minimize this variation. With an optimised set of parameters, one can maintain the variation within a 5% interval (see Fig. 7). Note that with acute corners a strictly uniform liquid argon/converter ratio can be realised. Note also that the "uniformity" optimisation is rather sharp: changing the (mean) liquid argon gap from 1.9 mm to 1.95 mm deteriorates in a visible way the uniformity (from 4% to 5%).

The effect of this non–uniformity of the material seen by a shower is considered in Section 2.5. The fact that the electric field around the corners is not uniform and has on average a lower value compared to the value in the straight sections could be a further source of non–uniformity. This point is also addressed in Section 2.5. In Fig. 8, we show the electric field strength as a function of the position in the cell. The bending radius of 3 mm is chosen such that nowhere the electric field will exceed the value of the flat section by more than 10%. This precaution was taken to ensure safety of operation. Assembly of the calorimeter with the required tolerances is based on the use of a support plate in which grooves of the desired accordion shape have been machined. Side plates and a segmented cover with the same grooves give the overall rigidity. No attempt has been made in the design of this first prototype to minimize the amount of dead materials around the active area.

2.3 Electronics Readout for the Prototype

The prototype, as described in the previous section, has a two–fold longitudinal segmentation with connections to the front and back faces. Three adjacent strips are connected together, thus forming towers with a cross–section of 2.5 cm x 2.8 cm (Fig 9). Since the projected transverse dimension of the accordion is also 2.8 cm, a particle on a straight track, e.g. a muon, will always give a signal shared by two adjacent towers. With the liquid argon gap chosen (1.9 mm), the drift time of electrons in pure argon is close to $t_d = 400$ ns, and even somewhat larger in the curved sections where the gap is larger, and the field, on average, smaller. For high–rate operation, as at the LHC, the occupancy time of the electronics has to be reduced considerably by 'clipping' the signal. This is usually done by shaping the preamplifier output with a bipolar weighting function, of much shorter characteristic time than t_d. For this procedure to work, it is necessary that the transfer time from the detector to the preamplifier be fast, of the order of 10 ns or less for LHC. With the accordion structure, such a short time can be achieved, provided a preamplifier of low enough (resistive) impedance ($\leq 20\ \Omega$) is connected directly to each tower (see Section 4.). This requires electronics working at the liquid argon temperature [4].

One type of preamplifier we are planning to use is based on the design previously developed for HELIOS. Hybrid circuits are used with input Silicon FET's from Interfet. The design is shown in Fig. 10. In order to cope with 150 GeV showers from the SPS, a feedback capacitance as large as 22 pF is used. In the present situation, without transformer at the input, a very large FET at the input would be best suited, both for noise figure and for the rise time (small R). Some large FET's are actually fabricated by Interfet which would have suited our needs (80 pF capacitance). However a large enough batch of those elements with good performances was not available in time for this work. We will therefore use smaller input transistors (20 pF). In these conditions the input impedance is measured to be about 25 Ω at LAr temperature, thus introducing a first limitation to speed in the present set–up.

The prototype will also be equipped with 64 GaAs charge sensitive preamplifiers developed by members of the Milano group, experienced in the field of cold electronics for cryogenic particle detectors. The present design consists of a modified version of a preamplifier originally intended for operation at longer peaking times at Liquid Helium temperature [8]. GaAs was adopted for its favourable performances at cryogenic temperatures (Chapter 4.3).

The GaAs preamplifier [8] uses ten MESFETs in parallel reaching an input capacitance of 80 pF. The feedback network consists of a 22 pF capacitance paralleled with a 330K resistor (Fig. 11). The Equivalent Noise Charge ENC at 77 K for $C_d = 400$ pF is (for unipolar Gaussian shaping with 100 ns shaping time) 5500 electrons rms. Using bipolar shaping the ENC was determined to be about 10 000 electrons rms. The input resistance is 19 Ω. A rise time of 25 ns was measured. Integral non–linearity is 0.03%, and the power dissipation is 74 mW.

Since the beginning of this project, time has been too short to develop suitable shaping amplifiers with $t_p \approx 30$ ns, as needed for LHC. For practical purposes, we are going to use in a first test the shaping amplifiers of the HELIOS Uranium calorimeter. For these devices, $t_p = 90$ ns, which is a second limitation in speed for this set–up.

The intercalibration of the different channels of a liquid argon calorimeter is a well known procedure. The problem however becomes more difficult when one aims at a small constant term (below 1%) at high speed. In the prototype presented here, we are setting up a calibration system using precision capacitances of 22 pF, measured to 0.1 pF accuracy. In order to allow cross–talk studies, only 1 channel out of 3, in both longitudinal subdivisions, is pulsed at a given time. This is achieved by having the calibration elements on a vertical board, while the preamplifiers are organised by 8 on a horizontal mother board. We have verified, with one complete electronic chain, that the calibration system delivers pulses which are uniform to $\pm 0.25\%$. Concerning the electronic noise, a figure anticipated with the present device, if connected to fast electronics (t_p = 30 ns), would be around 30 to 50 MeV. Laboratory measurements with the present (slower) chain give significantly lower values ($\approx$ 5 MeV). Electronic noise therefore should not be a limitation in this particular set–up.

2.4 Test–Beam Set–up

In addition to the shaping amplifiers, we plan to use parts of the HELIOS calorimeter for the beam test. We will use the cryogenic equipment and the cryostat, and part of the hadronic section of the existing uranium calorimeter. The new set–up is shown in Fig 12. The uranium part has a section of 1.2 m x 1.2 m and a thickness of 2.5 interaction lengths. Its purpose is to provide some electron/pion signature and to serve as backing calorimeter for those electron showers which might leak slightly from the new prototype. Apart from the preamps, the readout chain is the same for the (new) electromagnetic part and for the existing hadronic part. The readout uses LeCroy 2281 peak sensing ADC's with their dedicated CAMAC processor. Data will then be treated by a CETIA station which has a 68030 processor, a buffer memory and tape writing and monitoring capability. Interfaces of those elements are organised in VME. Concerning the beam itself, in a first round we shall set up in the H6 beam of the North Area which delivers pions and electrons over a large momentum range. The standard beam equipment will be supplemented by trigger counters and drift chambers from the UA2 test beam facility.

2.5 Simulation of detector performances

We mentioned in the first section that, for an optimized set of parameters, the ratio of argon to passive materials, as seen by perpendicularly incident muons, can be made uniform to ± 5%. The ability of the design described here to be a candidate for LHC electromagnetic calorimetry – with a small enough constant term – rests on the hypothesis that the shower spread will average out this modulation to an acceptable value (below 1%). This hypothesis needed to be supported by detailed studies.

For that purpose an effort was organised to simulate, with the best present knowledge of electromagnetic shower behaviour, the response of electrons and photons in the proposed structure [9]. The simulation undertaken was organised in the GEANT framework, which allows to deal with rather complex geometric structures but requires special care to economize computer time.

In a first round of simulations, the total dE/dx of charged tracks in the liquid was used as response, without including charge collection. The first test made was to simulate muon tracks through the calorimeter. The average value of the charge collected, as a function of impact position, is shown in Fig. 13, together with the analytical calculation of the argon to other material ratio. The good agreement between the two independent approaches is a test of the reliability of the calculations. Shown in the same figure is the response to muons at 20 mrad incidence. In this case the modulation is significantly reduced, because "corners" no longer align themselves with the track.

Showers of 40 GeV electrons were simulated, using cut–off parameters of 1 MeV (electrons) and 0.1 MeV (photons). The display of such an event is shown in Fig. 14. The energy distribution of events all impinging at the same point is shown in Fig. 15. The energy released in the liquid is on average 6.955 GeV, i.e. 17% of the shower energy. The width of the distribution is 0.882 GeV (rms) which, if attributed to a resolution behaviour like $k/\sqrt{(E)}$, corresponds to k = 8.3%. By doing similar simulations at different impact points in the structure, we then evaluated the modulation remaining for electromagnetic showers. The result obtained is shown in Fig. 16. The rms distribution of the 5 points considered is 0.86%. With points randomly distributed over the cell one can anticipate a slightly smaller spread. The next step was then to simulate the main features of the charge collection readout. For this calculation, each elementary charged track segment, with its energy release, position (relative to electrodes) and direction was stored on disk or tape. In the simulation we calculated the signal induced on the nearby electrode by a localised energy deposition moving in the electric field. It included a field map as shown in the first section, and a dependence of electron velocity on the field. Convolution with the bipolar shaping was also incorporated (see Ref. 9

for more details). The result is presented as a ratio, shower by shower, of the charge response of the electronics divided by the energy released by the shower in the liquid (Fig. 17). The ratio rms/peak position of this distribution is 0.29%. This value shows that no large effects are to be expected from the field inhomogeneities and readout features.

The position resolution has also been studied in the simulation, especially in the direction perpendicular to the accordion folds. Using towers of 3 cells (as shown in Fig. 9) we get the shower profiles presented in Fig. 18. Depending on the electron position (centre or edges of the tower) the charge is distributed over two or three towers. A 'nonet' of three by three towers is therefore considered adequate for position measurements. At 40 GeV, preliminary estimates give an accuracy of about 0.6 mm. Work is in progress to estimate the effect of electronic noise and pile–up of minimum bias events.

In summary, we view this first prototype as a tool to evaluate the feasibility and performance of this newly proposed 'accordion' technique. The electronics that we shall use in the first test is the fastest which could be made available to us at the present time. Its speed is however below the intrinsic speed of the accordion itself, and not adequate for LHC operation at $L = 2 \times 10^{34}$ cm^{-2} s^{-1}. Developing faster and radiation hard electronics is one of the topics which we wish to consider in the coming year. This topic is discussed in Chapter 4. Requests for test beam time to test this prototype equipped with new electronics are given in Chapter 7.

3. DESIGN STUDY OF A LARGE ACCEPTANCE CALORIMETER FOR THE LHC

3.1 Introduction

As part of our proposed programme, we wish to study the concept of an LHC LAr calorimeter with large rapidity coverage. We assume that the electromagnetic and hadronic calorimeter sections will be included in a single cryostat for the central rapidity region. The forward calorimeters will be considered at a later stage. For this engineering study, we plan to use powerful software tools, integrating engineering programmes (finite element analysis, thermal analysis) and particle tracking in one CAD platform [7]. As a starting set of parameters for the study of the barrel part of the calorimeter, we consider:

- full coverage in azimuth;
- polar angle coverage from 25° to 155° corresponding to a rapidity coverage close to ± 1.5 units;
- entrance wall of the calorimeter cryostat at a radius of 130 cm;
- an electromagnetic section of 27 radiation lengths depth corresponding to a physical thickness of about 50 cm;
- start of the hadronic part at a radius of about 180 cm and with a thickness of at least 8 λ for normal incidence.

While these parameters help to set the scale for the initial discussion, we will of course –as part of our design study–reevaluate them very carefully as well as investigate the degree of segmentation required for the electromagnetic and hadronic calorimeters.

3.2 Electromagnetic Calorimeter

A design based on the accordion technique will be pursued. We consider maintaining, over the full barrel calorimeter, a transverse segmentation of the order of 0.02 to 0.03 in both azimuth and rapidity. This corresponds to cell dimensions of 3 to 4 cm in both directions, a value which is matched to the Moliere radius of a lead/LAr sandwich (layers of 2 mm of lead and 4 mm of liquid argon). The study will allow the possibility of having a longitudinal segmentation of the 27 radiation lengths into 2 to 3 compartments. The R&D project on the electromagnetic calorimeter will concentrate on a series of subjects described in the following paragraphs.

Pointing tower structure

The prototype described in Chapter 2 is constructed with a non–pointing geometry. This will have to be modified to satisfy the requirements of cells pointing to the interaction region, both in the azimuthal and the rapidity directions. A detailed study of the implications of various possibilities will be made, like constant absorber thickness, constant liquid argon gap, constant angle of the accordion waves. For polar angles away from 90°, the mechanical structure depends strongly on the orientation of the accordion waves (parallel or perpendicular to the beam direction) as illustrated in Fig. 19. The partition of the calorimeter into sub–elements of reasonable size will be studied in connection with the question of the possible appearance of cracks, and of the design of supporting structures. As in the prototype, we foresee that the front–end electronics will be directly attached to the detector and the mounting and cabling of the cold preamplifiers will be studied.

Material and fabrication studies

The absorber of the present prototype is made of a composite of a 1.8 mm lead sheet plated with two 0.1 mm stainless steel sheets. Further tests of this technique need to be done to adapt to new geometries and to match the requirements of large scale production. In parallel, other materials will be investigated. The composition and fabrication of the anode readout plane will also be studied. In particular, additional studies will be necessary, if the electromagnetic compartment were to be split into three sections. The two outer sections can be read directly from the front and the back of the calorimeter but the connection of the inner section would need a more complex multi–layer circuit.

3.3 Hadronic Calorimeter

The principal performance requirements of a hadronic calorimeter are good hermeticity, an energy response similar for hadrons and photons and a signal response adapted to the LHC, operating at luminosities of up to 2×10^{34} cm^{-2} sec^{-1}. We consider the following starting parameters, but stress the need for considerable simulation work before more definite parameters can be obtained:

- tower size: 0.1 x 0.1 in azimuth and rapidity (i.e. 20 x 20 cm^2 at two metres from the interaction point);
- lead or iron plates or possibly composite structures as absorber with the aim to approach compensation;
- a ratio absorber/liquid argon of ~ 5, implying a calorimeter depth of approximately 170 cm. The inner radius of the hadronic calorimeter would be at about 180 cm and the outer radius at about 350 cm. The resulting weight of such a barrel calorimeter would be ≈ 250 tons/m length.

Readout of a hadronic calorimeter

High–rate capability is an especially severe requirement for the hadronic calorimeter for which the size of the cells implies a large capacitance, typically of the order of 10 nF. This large value, together with the preamplifier input impedance as well as the inductances associated with cabling and connectors, may imply a long charge transfer time (see Chapter 4).

Several methods may be used to reduce this transfer time. In one approach, adopted by the D0 and UA1 collaborations [10], the effective input impedance of the preamplifier is reduced by using several input FETs in parallel. Alternatively, ferrite core transformer can be used [4] to match the detector capacitance to the preamplifiers. This solution has many attractive features but cannot easily be used in strong magnetic fields.

A third, interesting approach reduces the effective detector capacitance through a different connection scheme for the electrodes [11]. This is shown in Fig. 20; the traditional scheme with all signal gaps connected in parallel is indicated in Fig. 20a. In Fig. 20b, an alternative scheme shows the gaps connected in series. The gap currents are not directly summed but the average signal is delivered into a much higher input impedance. Since this connection mode performs the same impedance transformation as a ferrite core transformer, it has been called electrostatic transformer (EST). As an example, a typical hadronic tower with 40 gaps of 250 pF each has a total capacitance of 10 nF, if all gaps are connected in parallel. In contrast, if the stack is structured in 8 parallel sets of 5 gaps each in series, the capacitance will be 400 pF. The number of gaps in series plays the same role as the turn ratio in a ferrite core transformer.

The EST idea has been tested in an aluminium mock–up [12,13], realized as a matrix of 9 adjacent towers of 15 x 15 cm^2 in cross–section. Each tower had two subsections with a transformer ratio of 5, but the model allowed variation of this ratio. The signal was collected by the central tile of each subsection (Fig. 21). As expected, fast rise times were observed and most importantly, results indicated that the performance of the towers is quantitatively predictable from a few geometrical parameters including absorber and liquid gap thicknesses, transformer ratio and spacing between neighbours. The performance is degraded primarily by cross–talk effects between adjacent towers. This is induced by differences in the ionization current in the gaps read out in series. However, this effect cancels to a large extent when summing over adjacent cells. The detailed agreement of all the electrical measurements made on the small mock–up with calculation shows that computational techniques such as SPICE simulation, can be used to help in designing a real tower.

A rather detailed simulation study of electromagnetic and hadronic shower development inside such an EST structure has been performed to quantify these cross–talk effects [13]. Results show that for cell sizes of 15 x 15 cm^2 in the hadronic section and 5 x 5 cm^2 in the electromagnetic compartment –which are smaller than the size needed to fully contain the shower energy– the natural shower fluctuations are larger than the additional fluctuations induced by the EST structure. This appears to hold for relatively high transformer ratios, like 4 in the electromagnetic section and 10 in the hadronic one which would provide a substantial reduction in detector capacitance.

Present Ideas on the Structure

We plan to study a hadronic calorimeter which combines the accordion structure and the EST readout. A schematic transverse section of a possible arrangement is shown in Fig. 22. The barrel calorimeter is split into several sections. The full azimuth is divided into 64 wedges.

The wedges will be subdivided in depth, possibly into two modules each (4 λ deep). Because of the accordion shape, small azimuthal gaps can be tolerated between modules without introducing significant cracks.

Each module would be built of 2 sheets of 5 mm stainless steel on the outside and 9 sheets of 1 cm lead inside. These 11 sheets define 10 gaps, 2 mm thick, for the liquid argon (see insert of Fig. 22). The steel plates are at ground potential and the lead plates are segmented following the geometry of the readout towers. The high voltage to produce the electric field across the LAr gap is applied via resistors to metallized insulating layers glued on the steel and lead sheets, such that the EST readout can be implemented. For each two sections of a module the 5 gaps on the left side (right side) can be connected in series, and the two sides in parallel. The capacitance of a section of a module is then about 400 pF like that of an electromagnetic section.

The two sections of a module can be read out through very short connections to preamplifiers located directly at the front and the back of a module. Studies will be performed on the mechanical rigidity of a self–supporting module incorporating the pointing geometry. The cladding with other absorber materials (for example, polyethylene) will also be considered, should further studies establish improved compensation for such configurations.

R&D Programme

1. for electromagnetic calorimetry:

We expect that the first prototype test of Summer 1990 will demonstrate the feasibility of the accordion scheme and that the results will suggest further tests. Furthermore, the development of pointing towers in the accordion geometry must be accompanied by dedicated tests. It would also be interesting to test the minimum practical thickness of the liquid argon gap. For these reasons, we expect to initiate the construction of a new prototype at the beginning of 1991.

2. for hadronic calorimetry:

We have mentioned a number of points requiring further studies before the design of a LHC calorimeter can be attempted. We propose to test the basic ideas exposed here. We plan to built a full size prototype representing a sector of a barrel calorimeter. We consider a module of about 4 x 4 towers and of full depth, with the electrodes connected using the EST scheme.

At the same time a detailed engineering study of a complete barrel (including support, dead space, connections, assembly scheme) will be pursued.

We plan to submit an Addendum to this Proposal presenting the results of the Summer test together with a detailed engineering description of the new prototypes at the end of 1990.

4. FRONT END ELECTRONICS

In this chapter we briefly address the principal parameters of the preamplifier and shaping amplifier, which determine the temporal response of the detector and signal processing chain.

The characteristic signal forms, before and after shaping, are shown in Fig. 23. The triangular shape of the induced current corresponds to uniform energy deposition in the liquid gap and starts immediately after the energy deposition. For the high–energy showers and for the geometries we have considered (as well as for the 'classical' ones), the approximation of uniform energy deposition in the gap is valid. In principle, therefore, the energy of the shower can be measured by integrating the current pulse over time intervals, much shorter than the duration of the pulse, determined by the drift time t_d.

In practical devices, the following parameters will limit the temporal performance [5]:

– the transfer time τ of charge from the detector electrodes to the preamplifier;
– the required signal–to–noise ratio;
– the performance of the components needed in the preamplifiers and shapers.

We address these points in the following sub–sections and indicate the topics on which we plan to concentrate our R&D efforts. The signal–to–noise performance, in particular, will be a balance between the acceptable 'pile–up' noise and the electronic noise of the signal processing system. However, the relatively high–energy deposits to be studied at the highest LHC–luminosities allow relatively high absolute levels of noise.

4.1 Charge Transfer

Our brief discussion follows [5]. Three parameters determine the transfer speed:

C... capacity of the detector elements at the preamplifier input;
L... inductance of the detector elements at the preamplifier input;
R... input impedance (resistive) of the charge sensitive preamplifier.

These elements form a series circuit for which the critical damping conditions are satisfied for $R = 2\sqrt{L/C}$. In that case, the charge transfer time τ (10% to 90% rise time of the charge signal at the preamplifier input) is found to be:

$$\tau = 4 \cdot \sqrt{LC} = 2\,RC.$$

For a given detector capacitance C, fast charge transfer with adequate damping requires small values of both R and L. As an example, we indicate the values for the prototype discussed in Chapter 2: $C \approx 400$ pF, $L \approx 10$ nH and therefore $\sqrt{LC} = 2$ ns, i.e. $R = 10\ \Omega$! For these detector parameters, the response can indeed be very fast, provided the preamplifier input impedance is low enough. This is a major limitation as will be discussed in the following section.

4.2 Preamplifier Limitations

Viewed from the detector, a charge–sensitive preamplifier is seen as a capacitance with a value $A \cdot C_f$ (A denotes the low–frequency open–loop gain, C_f the preamplifier feedback capacitance) in series with a resistive impedance with value $C_p/(g_m C_f)$. In this relation C_p defines the dominant pole of the response, and g_m is the input stage transconductance. The output signal is essentially Q/C_f where Q is the charge collected by the electrodes. This relation indicates possible handles to achieve a small input resistance. In practical circuits the feedback capacitance C_f has to be an order of magnitude lower than the detector capacitance C, in order to achieve a net gain of the preamplifier (see however section 4.4 for a different approach). The feedback capacitor is also limited by the driving capability of the output stage for a given power dissipation. Furthermore, the pole capacitance C_p needs to exceed a certain value, such that the pole of the next stage does not provide a limitation. The transconductance of the input FET can be increased by engineering special geometries of the FET or by paralleling several FET's in the input stage (see Chapter 2), albeit at the price of higher power consumption. The analysis of these parameters indicates that today's Si FET technology will typically achieve values of $R \sim 20\ \Omega$.

4.3 GaAs Front–End

At room temperature, GaAs MESFETs are characterized by a low level of white noise at low power dissipation, but show large 1/f noise and a high gate leakage current. For these reasons they have been used particularly at frequencies in the GHz range, and become of interest at very short shaping times. The situation becomes much more favourable at cryogenic temperatures. The energy of dopant impurities in GaAs is small, preventing freeze–out of carriers, even at temperatures as low as 4 K. The gate leakage current decreases exponentially with decreasing temperature (Fig. 24) and 1/f noise decreases strongly (Fig. 25). The white series noise, limiting the resolution at short shaping times, has a very much lower dependence on temperature due to hot electron effects: at 100 ns peaking time the Equivalent Noise Charge is measured to be practically independent of temperature. The radiation resistance may also be quite favourable (see Chapter 6).

The static and noise performances of GaAs devices at low temperatures have been investigated extensively with cryogenic detectors as primary goal [8,14–18]. The first charge–sensitive preamplifier using exclusively GaAs MESFETs was discussed in [18], and a subsequent version, matching detector capacitances of 80 pF, was described in [8]. The low Equivalent Noise Charge (90 electrons rms at 77 K), low power dissipation (29 mW) and fast speed (15 ns) with C_f = 10 pF and for zero detector capacitances are the basis for the realization of high performance front–end electronics for particle detectors operating at cryogenic temperatures (Fig. 26).

In view of these attractive features, we decided to equip the e.m. prototype with 64 GaAs preamplifiers, especially developed for this application. Ten transistors in parallel at the input stage provide a fair degree of capacitance matching; the feedback capacitor is 22 pF. The performance of this preamplifier was described in Chapter 2.3.

It is our intention to develop the Si JFET and GaAs approaches in parallel for the time being. Further studies will determine whether monolithic versions are to be considered advantageous and/or realistic in the near future. Radiation hardness tests will also be completed.

4.4 An Alternative Approach

Other solutions under study aim to reduce the cold electronics. As a minimum, a single transistor follower, either a Si JFET or a GaAs MESFET, would be mounted in a common gate mode. The charge–sensitive preamplifier would be located outside the cryostat and operated at room temperature. This solution has the advantage of lower power dissipation in the cryostat, but is characterized by increased noise and possibly larger cross–talk, requiring careful evaluation.

4.5 Shaping Amplifiers

Shaping of the signals following the preamplifiers is required to achieve:

- integration of the signal charge for a predetermined time to control the level of pile–up noise;
- selection of the brandwidth to optimize the signal–to–noise ratio;
- 'equal–area' shaping to ensure that the pile–up of signals produces on average no baseline shift, i.e. no apparent energy deposit.

We characterize the bipolar shaping by its peaking time t_p for a delta–current (i.e. a very short signal current), see Fig. 23. For triangular current pulses of duration much longer than t_p, the peaking time for the shaped signal approaches

$$t_p \text{ (triangle)} \approx 2\, t_p\, (\delta).$$

The HELIOS shapers which we are going to use in the prototype tests, have a $t_p (\delta) \approx 90$ ns, not quite fast enough for very high luminosity operation. As indicated in Fig. 1, for luminosities approaching 20 $nb^{-1}s^{-1}$, shaping times as short as $t_p (\delta) \sim 30$ to 40 ns could be envisaged in order to balance the pile–up noise contributions with the electronic noise. As an example, for $t_p (\delta) = 30$ ns, approximately 17% of the total charge produced is measured. This value corresponds to a drift velocity in liquid argon of $v_D = 5$ mm μs^{-1} and a drift gap of 2 mm. The sampled charge would increase to approximately ≥ 30% if the drift velocity were increased to $v_D \sim 10$ mm μs^{-1} with e.g. the addition of methane. The effective electronic noise, expressed in terms of energy deposit in the calorimeter which would be observed with such a fast shaping is estimated to be 40 MeV/e.m. tower for pure LAr and approximately 20 MeV/e.m. tower for 'fast' LAr.

We are presently evaluating the feasability of developing the shaper function in monolithic form.

4.6 Dynamic Range

The total noise (pile–up and electronic) and the maximum expected energy deposit in a detector element set the scale for the dynamic range. At the LHC, electromagnetic energy deposits could be as high or even larger than one TeV, if e.g. very heavy Z's were to exist, observed in the decay mode $Z' \rightarrow e^+e^-$.

Based on the previous noise discussion (20 to 40 MeV/e.m. tower) a dynamic range approaching 10^5 will be needed. While such a requirement does not pose any fundamental problems, the practical consequences, such as output voltage for minimum and maximum energy deposits and power consumption of the preamplifiers require very careful engineering studies.

Appraisal of the engineering issues of these preamplifiers, their design and subsequent system tests will be pursued with high priority.

5 SIMULATION STUDIES

5.1 Introduction

Simulation studies for the 'accordion' geometry were presented in Section 2. Here we present first results obtained within the framework of long term simulation studies. The aim is to simulate electrons, hadrons and jets, and to study their detection properties (resolution, linearity, ratio of electromagnetic to hadronic shower response, e/h) for several calorimeter configurations. These simulations will also be used in the future to look into other aspects of calorimeter design, like hardware and software compensation tuning, e.m. and hadronic granularity, lepton isolation, consequences of the granularity at the trigger level.

5.2 Geometry

So far, we have simulated two barrel configurations, with cylindrical Lead/Liquid Argon layers. The radial configurations in these simulations are as follows:

a. *Calorimeter with identical sampling for e.m. and hadronic compartments*
   - a 'cryostat', 0.7 X_0 Fe and 4 cm Air at R = 150 cm, followed by
   - 10 λ of alternating layers of 0.3 cm Pb and 0.4 cm LAr
     (522 double layers, up to R = 521 cm).

b. *Calorimeter with different sampling for e.m. and hadronic compartments*
   - A 'cryostat', 0.7 Xo Fe and 4 cm Air at R = 130 cm;
   - 27 X_0 of alternating layers of 0.3 cm Pb and 0.4 cm LAr
     for the electromagnetic compartment corresponding to 48 double layers and a depth of 34 cm;
   - 10 λ of alternating layers of 1.0 cm Pb and 0.4 cm LAr for
     the hadronic compartment, which yields 160 double layers and a depth of 224 cm.

While the first set–up corresponds to a calorimeter with unrealistically fine sampling, the second one represents a more practical version, which should give results comparable to those achievable in an experiment.

5.3 Simulation Tools

The calorimeter performance was studied through full electromagnetic and hadronic shower simulation. For the simulation, the GEANT 3.14 package [19] was used interfaced to JETSET 7.2 [20] for the jet fragmentation and running GHEISHA [21] for the hadronic showering. The particles were followed individually down to a very low threshold (11 keV) and the energy deposition in the active layers was recorded as an energy measurement*. Saturation effects ("Birks law") were taken into account reducing the energy deposition signal by the Birks factor. A time–of–flight cut TOFMAX = 150 was set, corresponding to a 150 ns gating time. The simulations were performed on a CRAY, where typically the CPU time needed was 1 s/GeV.

5.4 Calibration

For the calorimeter with the two different samplings, a calibration factor α was determined, to combine the signals of the two sections for hadrons:

$$S_{TOT} = S_{EM} + \alpha \cdot S_{HAD},$$

where S_{TOT} is the signal that provides the particle energy measurement, S_{EM} and S_{HAD} are the energy deposition signals in the e.m. and hadronic sections respectively. The calibration factor α is weakly energy dependent, and is obtained from a linear fit $\alpha(S_{TOT})$ for particles with energy larger than 25 GeV, where S_{TOT} is the signal determined with a constant calibration factor. No weighting techniques [22] were used, which would be possible with fine longitudinal granularity.

5.5 Results

The results for resolution, linearity and e/h ratio are presented in Fig. 27 for the homogeneous sampling calorimeter and in Fig. 28 for the one with two samplings. For the homogeneous sampling (Fig. 27), we obtain that the ratio e/h is > 1, particularly pronounced at low energies. This affects the jet resolution also at high energy, because jets have a substantial electromagnetic fraction (1/3 on average), and the particles in the jet have only a fraction of the original jet energy. The resolution is in the expected range, worsening at high energy ($\geq$ 70 GeV) where also the linearity and e/h are noticeably changing again. The resolution shown for hadrons corresponds to $(33 \pm 4)\%/\sqrt{E} + (3 \pm 1)\%$ with E in GeV as indicated by the curve in

* [the GEANT datacards were tuned for stable results and optimum speed. We used DCAY 1 / MULS 1 / PFIS 1 / MUNU 0 / LOSS 2 / PHOT 1 / COMP 1 / PAIR 1 / BREAM 1 / DRAY 0 / ANNI 1 / HADR 1 except for Pb, where we used DRAY 1 and LOSS 3 (Landau fluctuations below cut off) and the δ–ray and Bremsstrahlung cuts were set to 1 MeV, tracking parameters were DEEMAX = 0.02, EPSIL = 0.02 cm while the maximum step allowed in a medium was chosen as 1/10 of its radial thickness]

Fig. 27. Jets show a somewhat worse energy resolution than single charged pions, due to their electromagnetic (π^0) component since the calorimeter is not compensating.

For the inhomogeneous sampling (Fig. 28), we show the resolution coefficients obtained with the energy dependent calibration coefficient. The resolution can be described (solid curve) by $(45 \pm 3)\%/\sqrt{E}$ + $(3 \pm 1)\%$ with E in GeV. The linearity and e/h ratio are evaluated with a single constant factor obtained by averaging over the high energy points. Note that the adopted calibration procedure only minimizes the hadronic resolution leaving the absolute response of the electromagnetic compartment unchanged and therefore the ratio e/h unconstrained. The hadronic and jet resolutions are generally worse than in the homogeneous case, caused by the coarser sampling in the hadronic section.

The errors we quoted are only statistical, from the simulation. However, systematic uncertainties are present, due to the models used in the showering [21]. It will be possible to test the reliability of the calculations in comparing them with existing measurements in an Uranium–LAr calorimeter and Pb/Fe–LAr (H1) calorimeter. However, technical problems about hadronic showering in fissionable materials have to be solved first within the simulation packages. Other calorimeter configurations are being studied as well, including hybrid geometries (for example a Pb/LAr electromagnetic section followed by a Pb/Scintillator hadronic section).

5.6 Future Simulation Work

The design studies outlined in Chapter 3 will have to be complemented and optimized by a large effort in shower simulation work. In particular, details of a pointing accordion tower structure will have to be studied with electromagnetic shower simulations as described in Section 2.5 for the first prototype. The response to hadrons and jets will be investigated for the specific hadron calorimeter configurations considered. As already mentioned, the tuning of the e/h response ratio as a function of the absorber material(s) is a very important aspect which will be studied systematically. In addition, a broad programme of simulation studies of general calorimeter design parameters such as granularity and coverage is undertaken in order to address the LHC physics requirements.

6. SELECTION OF RADIATION RESISTANT COMPONENTS

One – and not the least – of the formidable challenges posed by LHC–experimentation, is the development of detectors, which show adequate radiation resistance. We believe to have a reasonable understanding – within a factor of two to three – of the radiation levels which we will encounter [23]. This assumes that the principle radiation load will be caused by particles originating in p–p collisions.

Typical integral radiation levels for $L = 2 \times 10^{41}$ cm^{-2}y^{-1} (10^7s at 2×10^{34} cm^{-2}s^{-1}) are given in Table 2. In addition to the radiation load produced by the low energy π^{o}'s, special attention should be paid to the particle spectra in the hadronic showers. Of particular concern is the copious flux of neutrons created along the shower and of the albedo neutrons which are emitted in the backward direction through the front face of the calorimeter. As an example, the number of albedo neutrons from a lead calorimeter is estimated to be of the order of 2×10^{13} cm^{-2}y^{-1} for a total luminosity of 2×10^{41} cm^{-2}y^{-1}. Monte–Carlo calculations and comparison with data show that the choice of calorimeter materials is very important and that the presence of hydrogenated materials has a major consequence on the neutron flux. The number of neutrons created by hadronic showers have been measured at SPS in a dense iron stack [24]; experimental data obtained in various targets [25] show that the total number of neutrons outside a cylindrical block (10.1 cm diameter 60 cm long) is uniformly distributed and may be parametrized as [Fig. 29]:

$$N = 0.1\ (A + 20)\ (E - 0.12)$$

[A = atomic number, E = hadron energy in GeV],

except for U^{238}, for which $N = 50\ (E-0.12)$.

One reason for our choice of the liquid argon calorimeter technique is its relatively good resistance to radiation. Materials for the construction of such a calorimeter exist which have adequate radiation stability as shown in Table 3; getting to firm conclusions is part of our proposal. While liquid argon itself is very radiation hard, the addition of dopants, such as methane or allene, needs to be better understood as far as stability under irradiation is concerned. Another concern is the radioactivity induced by neutron activation. Extrapolation of the D0 estimate of the noise component due to the use of uranium [26] shows that an induced radioactivity comparable to the natural uranium radioactivity would lead to a 10 to 20 MeV effect in the electromagnetic section. Activation tests of materials including thermal neutron production of Ar^{41} will be made at existing neutron sources.

The remaining critical parts are the readout amplifier, shaping amplifier, the decision logic, data storage and digitization. The solution studied is to use first stage amplifiers located on the calorimeter at liquid argon temperature; Si JFET technology can be used, GaAs will also be studied since it may have better radiation resistance and lower power dissipation. Shaping amplifier, decision logic, data storage and digitization should be located away from the calorimeter in a lower radiation environment. Such an architecture is felt to be feasible. (See discussion in section 4). Values for the radiation resistance of front–end components presently available are summarized in Table 4.

In addition to radiation damage studies on detector components, extensive calculations on the expected radiation levels will be needed. Several elements need to be introduced into simulation codes to ensure realistic evaluations:

- realistic detector geometries with a complete description of all the detector materials;
- compilation of particle production and absorption cross–sections. Particular attention will have to be paid to thermal and epithermal neutron fluxes.

These simulations will be carried out by members of this collaboration. The work will be based on already existing simulation codes, such as Fluka 87 and EGS4, but major improvements, particularly on the low–energy neutron transport, are required to obtain reliable results.

7. MILESTONES, RESPONSIBILITIES AND REQUESTS

Milestones:

1. July 1990: First Accordion Test;
2. October 1990 (ECFA Meeting Aachen): first engineering sketches of the mechanics of an e.m. and hadronic calorimeter with large rapidity acceptance;
3. End of 1990: clarification of design of next prototype;
4. Spring 1991: start construction of next prototype;
5. May 1991: new fast electronics (Si preamplifiers, GaAs preamplifiers, fast shapers). Total of about 500 channels;
6. Second test of old accordion with optimized fast electronics chain;
   Dopant test;
   These tests would be carried out in the HELIOS cryostat, in essentially the same configuration as that used for the summer 1990 test.
7. February 1992: new prototype built; preparation for beam tests;
8. April 1992: beam test of new prototype.

Responsibilities:

Annecy (LAPP):

- participation in the design studies of a large acceptance calorimeter. Particular interest in the test of the EST concept;
- potential interest in participation in signal processing studies (e.g. trigger aspects and data acquisition);
- calorimeter simulation.

BNL:

- participation in the design of the signal processing.

CERN:

- participation in design studies of a large acceptance calorimeter;
- participation in certain aspects of the signal processing (triggering);
- calorimeter simulation;
- test beam infrastructure;
- participation in radiation tests.

Milano:

- responsibility for the GaAs front–end;
- radiation tests on the front–ends;
- radiation level calculations;
- calorimeter simulation;
- the possibility of involvement in cryostat design.

Orsay:

- participation in the design studies of the large–acceptance calorimeter;
- responsibility for new fast front–end and shapers;
- calorimeter performance simulation;
- participation in radiation tests.

Joint Responsibilities:

- Summer 1990 test;
- construction of the next prototype (personnel and money, with the exception of BNL);
- future beam tests.

Requests for activities during 1990 and 1991

In the following we summarize costs for the first accordion test (1990); we also present an estimate for the programme outlined for the period Fall 1990 to end of 1991. We discuss the test beam requirements, computing resources and engineering support.

1. Accordion Test 1990

		Cost (KSFr)
Mechanical construction (incl. special tooling)	CERN	90
Kapton readout boards	CERN	16
	ORSAY	35
Preamplifiers (Si)	BNL	10
(GaAs)	MILANO	10
Installation	CERN	10
(travel costs for staff not included)		
		171

2. Accordion Test 1991

New Fast Preamps (Si)	ORSAY	20
(GaAs)	MILANO	20
New Intermediate Amplifiers		20
Fast Shapers (hybrid or monolithic)	ORSAY	100
New Readout Electrodes (3–fold longitudinal division)	CERN	40
DAQ	LAPP	30
New Signal Cables	CERN	30
Operation of Test (LAr, Regie, beam instrumentation)		40
		300

3. Construction of New Prototypes

(Estimates: firm figures by end 1990)

E.M. Prototype

Mechanical prototypes	40
Construction of e.m. prototype	200
Kapton readout boards	100
Calibration system, cables, connectors	20
300 channels of readout electronics	90
Regie (1 man–year)	60
	510

Hadronic Prototype

Mechanical Prototypes	40
Construction of hadronic prototype	500
Readout boards (100 m^2) plus High Voltage distribution	40
Supports, handling devices	50
Tooling, contingency for mechanics	100
Preamplifiers (including GaAs and Si development)	40
Monolithic GaAs preamplifiers	60
Regie (1 man–year)	60
	890

These costs do not include the cryostat. We are investigating the possibility of obtaining a suitable one on loan.

4. Test Beam Requests (1991)

We request to have the beam line in vacuum up to the position of the experiment.

Test 1: performance of e.m. prototype with fast electronics	15 days
Test 2: Tests with CH_4 (including the response of the HELIOS U/LAr hadronic modules)	5 days
Test 3: Tests with other dopants (if laboratory tests provide positive indication)	5 days

5. Computer Time

Our estimate is based on the computer usage for simulation during the first half of 1990, indicating that we will need 10 000 hours (IBM equivalent) to be shared as follows:

CERN	3500 hours
Outside Institutes	6500 hours

6. Engineering and Technical Support

We have developed our programme for 1990 and 1991 after indications that the engineering and technical support would be available in the collaborating Institutes such that the sharing of responsibilities as shown above can be respected.

7. Engineering Infrastructure

In Chapter 3.1, we emphasized the need for a new level of integration of simulation tools (e.g. GEANT) with mechanical CAD platforms. We are convinced that a timely preparation of the LHC experiments will require the preparation of such integrated engineering platforms. Furthermore, in view of the international nature of the collaboration, we perceive that it would be most advantageous to coordinate the procurement of these platforms in the National Laboratories and at CERN. A network of integrated platforms across Europe will be of great use and we ask the Management of the European Laboratories and of CERN to consider steps in this direction.

References

[1] P. Jenni, in Proc. ECFA Study Week on Instrumentation Technology for High-Luminosity Hadron Colliders; E. Fernandez and G. Jarlskog ed., CERN 89–10 (1989) 69.

[2] C.W. Fabjan, in 'Feasibility of Experiments at High Luminosity at the Large Hadron Collider, J.H. Mulvey ed., CERN 88–02 (1988) 19.

[3] A Yamashita and K. Kondo, Physics Noise to Calorimetry at SSC, Proc. DPF Summer Study on the Physics of the Superconducting Supercollider, Snowmass, Co., 1986 (AIP New York, 1987), p. 365; G.O. Alverson and J. Huston, Estimating background noise in LAr detectors due to pile–up, ibid., p. 368;
P.T. Cox, Ref. 2, p. 25;
L. Fayard, presented to the ECFA Working Group on Calorimetry, May 1990.

[4] D. Gilzinger et al., the HELIOS Uranium Liquid Argon Calorimeter, in preparation.

[5] V. Radeka and S. Rescia, Nucl. Instr. and Methods A265 (1988) 228.

[6] A.L.A. Angelis et al., Evidence for the Compensation Condition in Si/U Hadronic Calorimetry Achieved by the Local Hardening Effect, CERN–EP/90–73.

[7] T. Adams et al., An Engineering Design Study of a Hermetic Liquid Argon Calorimeter for the SSC, submitted to Nucl. Instr. and Methods.

[8] A. Alessandrello et al., 'Low–Noise, Gallium–Arsenide Charge–Sensitive Preamplifier for Low–Temperature Particle Detectors', Proc. of IEEE 1989 Nuclear Science Symposium, San Francisco 17–19 Jan. 1990, to be published in IEEE Trans. of Nucl. Sci. 1990.

[9] M. Lefebvre, M. Pepe and G. Polesello, Internal Note CAL–No–002, 24 May 1990.

[10] C. Bacci et al., A Hybrid Charge Sensitive Amplifier for High Capacitance Detectors, UA1–TN 88–08 (1988).

[11] J. Colas, M. Pripstein, W.A. Wenzel, The Electrostatic Transformer, to be published in Nucl. Instr. and Methods.

[12] J. Colas, Speed of Response, Pile–up and Signal to Noise Ratio in Liquid Ionization Calorimeters. Contribution to the ECFA study week on Instrumentation Technology for High Luminosity Collider, Barcelona September 1989, CERN 89–10.

[13] J. Colas, W.A. Wenzel, Analytical description of an EST, LAPP–EXP–90.07;
J. Colas, Electrostatic Transformer Performances: Shower simulation, LAPP–EXP–90.08.

[14] D.V. Camin, 'Perspective in the Design of Low–Noise, Low–Temperature Front–End Electronics for Cryogenic Particle Detectors', Proc. of the E–MRS Symposium on Superconducting and Low–Temperature Particle Detectors, ed. G. Waysand (Elsevier–North Holland, Amsterdam, 1988) 217.

[15] D.V. Camin et al., Cryogenics 29 (8) (1989) 857–862.

[16] D.V. Camin, Nucl. Instr. and Methods A277 (1989) 204–210.

[17] A. Alessandrello et al., IEEE Trans. on Nucl. Sci. 36(1) (1989) 471.

[18] A. Alessandrello et al., Nucl. Instr. and Methods A289 (1990) 426.

[19] R. Brun, F. Bruyant, N. Maire, A. C. McPherson, P. Zanarini, "GEANT3", CERN–DD/EE/84–1.

[20] T. Sjostrand, "The Lund Monte Carlo for Jet Fragmentation and e^+e^- Physics", JETSET version 7.2, CERN/TH.

[21] H. C. Fesefeldt, "Simulation of hadronic showers", PITHA–report 85–02 RWTH Aachen.

[22] V. Korbel, Nucl. Inst. Meth. A 263 (1988) 70; H. Abramowicz et al., Nucl. Inst. Meth. 180 (1981) 429.

[23] D. E. Groom (ed.), Report of the task force on Radiation Levels in the SSC Interaction Regions, SSC Central Design Group Report SSC–SR–1033 (1988); G.R. Stevenson, Radiation Levels in an Idealized Calorimeter, presented to ECFA–LHC–Calorimeter Working Group; to be published.

[24] J. S. Russ et al., CERN/TIS – RP/89–02 (1989).

[25] J. M. Carpenter, Nucl. Instr. and Methods 145 (1977) 91.

[26] S. Aronson et al., Nucl. Instr. and Methods A269 (1988) 492.

[27] N.V. Klassen, J. Phys. Chem. 72 (1968) 1076; R. Holroyd, private communication.

[28] H. Schonbacher et al., CERN 89–12.

[29] Engineering Materials Handbook A. S. M. Inernational.

[30] T. Ekelof, Ref. [1], p. 361.

[31] H. F. Sadrozinski et al., Nucl. Instr. Methods A288 (1990) 76.

[32] P. Jarron, private communication.

[33] A. Stevens et al., Rad–Hard Electronics Development Program for SSC Liquid–Argon Calorimeters, ANL–HEP–CP 90–33 (1990).

[34] W. R. Dawes, Nucl. Instr. Methods A288 (1990) 54.

[35] R. Zuleeg, Proc. of IEEE 77 (3) (1989) 389.

[36] B. K. Janousek, J. Appl. Phys., 63 (1988) 1678.

Table 1: Typical Performance Parameters Achievable with LAr calorimetry (Pb absorber)

Radiation resistance	>> 10^5 Gy
Energy resolution electrons, photons hadrons (jets)	$\sigma_E/E = 9\%/\sqrt{E} + 1\%$ (or better) $\sigma_E/E = 45\%\ (50\%)\ /\ \sqrt{E} + 3\%$ (E in GeV)
Granularity (electromagnetic)	$\leq 3 \times 3$ cm^2 (corresponding typically to $\Delta\eta \times \Delta\phi = 0.02 \times 0.02$)
Position resolution (electromagnetic)	≤ 1 mm
Calibration stability and response uniformity	1% (or better)
Time resolution	< 15 ns (assign isolated minimum ionizing particle to the correct bunch–crossing)

Table 2 Dose or Fluence per Year (luminosity 2×10^{41} cm^{-2}) for Pb/LAr Calorimeter [23]
[Cylindrical barrel calorimeter with inner radius $r_i = 130$ cm]

	Total Dose [Gy] Neutron Fluence [cm^{-2}]	
Pseudorapidity	0.5	1.5
Radius [cm]		
130 (start of e.m. calorimeter)	2×10^3 2×10^{13}	3×10^3 3×10^{13}
180 (end of e.m. calorimeter)	2×10^2 3×10^{12}	2×10^2 8×10^{12}
265	1 2×10^{10}	0.2 2×10^{10}
350	1×10^{-2} 0.3×10^9	2×10^{-3} 3×10^7

Table 3 Radiation Resistance of Selected Materials Used in LAr Calorimeters

COMPONENT	RADIATION RESISTANCE	REFERENCE
Lead, Stainless steel	used in accelerator construction; adequate	
CH_4	10^5 Gy will decompose 25% of CH_4 in LAr/0.5% CH_4 mixture	[27]
Allene	expected to be similar to CH_4	[27]
Kapton	darkening at 10^8 Gy	[28]
Fibreglass	> 10^{20} neutrons/cm^2 $\geq 10^{11}$ Gy precise values may depend on manufacturer	[29]

Table 4 Radiation Effects on Selected Electronic Components

Type of component	Process	Quantity measured	Radiation	Radiation level for 10% change	Reference
Cascode amplifier	SOS	Noise spectrum	Co–60 γ	> 4 10^3 Gy	[30]
p– and n– transistors	Rad. hard. CMOS SOI SIMOS	Threshold voltage g_m	Neutrons 20 KeV γ	> 2 10^{14} n/cm^2 10^4 Gy nMOS 10^5 Gy pMOS	[31] [32]
JFET preamp	Diff. junction Si–JFET	Noise spectrum	Co–60 γ	> 10^5 Gy > 10^{14} n/cm^2	[33]
Transistors	Bipolar	h_{FE}	Neutrons	10^{14} n/cm^2	[34]
JFET	Diff. junction Si–JFET	Gate leakage current Threshold voltage	Cs–137 electrons, γ Co – 60 γ	10^{-9} A after 10^4 Gy (Si) 10^4 Gy (Si)	[34]
JFET MESFET	GaAs GaAs	g_m Threshold voltage	Neutrons Co – 60 γ	10^{15} n/cm^2 10^5 Gy (GaAs)	[35] [36]

Figure Captions

Fig. 1 Estimates (solid lines) of pile–up noise (left ordinate) as a function of the product of the peaking time t_p and the luminosity (bottom abscissa) for two different sensitive areas. The typical electronic noise, as realised in the HELIOS U/LAr calorimeter (dashed lines), as a function of t_p (right–hand ordinate and top abscissa) is also shown. The peaking time t_p describes the rise time of the detector–amplifier system to a δ–pulse at the input.

Fig. 2 Electron / pion response of an U/LAr calorimeter as a function of particle momentum and peaking time [4].

Fig. 3a Conceptual view of the 'traditional' ion chamber calorimeter readout with parallel electrodes.

3b Concept of the 'accordion' for ion chamber calorimeters.

Fig. 4 Artist's view of the accordion calorimeter.

Fig. 5 Tool developed for the forming of the accordion absorber plates.

Fig. 6 View of the four–layer Kapton readout electrodes. The hatched are is covered with a resistive layer (~ 10 KΩ); the dark area indicates Cu–films not covered with the resistive layer.

Fig. 7 Total liquid argon thickness versus impact point for an optimized set of mechanical accordion parameters. The dotted lines delimit a ± 5% band.

Fig. 8 Electric field map in the accordion gap. The vertical bars give (in arbitrary units) the value of the electric field in the LAr gap. The region near an accordion bend, where the electric field is non–uniform, is shown.

Fig. 9 View of one tower showing the two–fold longitudinal segmentation; readouts are organized at the front and back of the calorimeter.

Fig. 10 Circuit diagram of the Si FET preamplifier.

Fig. 11 Circuit diagram of the GaAs preamplifier.

Fig. 12 Accordion prototype in the Helios cryostat, in front of the HELIOS hadronic sections.

Fig. 13 LAr radiation length seen by a minimum ionising particle as a function of impact point. Full circles correspond to normal incidence, open circles to 20 mrad incidence; the solid line gives the result of the analytical calculation for normal incidence and shows good agreement with the full simulation. The dotted lines delimit a ± 5% band.

Fig. 14 Display of a 40 GeV electron shower. All tracks are shown in (a). Only the charged and neutral tracks are shown in (b) and (c) respectively. In these figures, the cutoff energy for electrons and photons is 10 MeV.

Fig. 15 Energy distribution for 40 GeV electron showers in the LAr.

Fig. 16 LAr radiation length seen by a particle travelling perpendicularly to the calorimeter as a function of its impact point. The open circles show the response for 40 GeV electrons at normal incidence. The average response is normalized to the average LAr radiation length. The dotted lines delimit a ± 5% band.

Fig. 17 Distribution of the ratio of the energy deposited over the energy collected for 40 GeV electrons. Charge collection and signal shaping has been included in the simulation. The scale of the abscissa is arbitrary.

Fig. 18 Simulation of the position resolution. An r.m.s. accuracy of $\sigma \approx 0.6$ mm is estimated for 40 GeV electrons. Figs. a and c correspond to the electron incidence near a tower edge; Fig. b gives the distribution for central incidence. The abscissa is given in units of electronic channels.

Fig. 19 Transverse and longitudinal section of an e.m. calorimeter wedge.
a) accordion folds oriented azimuthally;
b) accordion folds oriented in polar angle.

Fig. 20 Comparison of the parallel and series connection (EST) of several gaps. In the parallel case, the equivalent current source is the sum of the current in each gap (p in total). The total capacitance seen by the preamplifier is the sum of the capacitance of each gap. A ferrite transformer of turn ratio p transforms this into a current <I> and a capacitance C/p. In the series connection, the equivalent current source is the average current of the gap currents <I>. The capacitance seen by the preamplifier is the gap capacitance divided by the number of gaps in series (s in total) C/s. This much smaller capacitance allows a faster readout. In a mixed scheme, some of the gaps would be connected in parallel and some in series. Note that in both cases energy conservation implies that the same signal to noise ratio is achievable.

Fig. 21 Aluminium model to study the EST pulse properties. The set–up consists of nine towers. Each tower is made up of two parallel sets of gaps; each set with 1 to 5 gaps. Aluminium tiles are 15 cm x 15 cm in area and 0.95 cm thick; sensitive gaps are filled with air; gap size is fixed at 2mm; tower spacing can be varied from 1.6 mm to 13 mm to study the influence of the coupling capacitance. The electrical schematic shown is used to simulate the pulse response of the model. The gap capacitance C is 100 pF; the coupling capacitance c is 15 pF.

Fig. 22 A possible layout for the barrel hadronic calorimeter, using the accordion concept.

Fig. 23 Characteristic signal forms in ion chamber calorimeters. The induced current resulting from the (uniform) charge deposit by ionizing particles traversing the chamber gap is shown in Fig. 23a. The bipolar impulse response of the detector signal processing is shown in Fig. 23b. For signals of the form shown in Fig. 23a, the output of the detector electronics is shown in Fig. 23c for shaping times shorter than the drift time of the charge. A detector with a three–lobe impulse response (Fig. 23d) would produce an output as shown in Fig. 23e, when driven by a signal of the form given in Fig. 23a [5].

Fig. 24 Gate leakage current of a GaAs MESFET as a function of temperature.

Fig. 25 Series noise at different temperatures in the realization of charge–sensitive preamplifiers.

Fig. 26 Equivalent Noise Charge as a function of detector capacitance for the preamplifier of Fig. 11 at 77K.

Fig. 27 Simulation results for a calorimeter with uniform sampling (see text). Top: resolution coefficient $\sigma = k/\sqrt{E}$ (%), for electrons (black circles), π^+ (white squares) and jets (black squares). Centre: linearity for electrons (black circles) and π^+ (white squares), calculated with respect to 10 GeV data. Black squares give the linearity for jets with respect to 10 GeV π^+. Bottom: e/h ratio.

Fig. 28 Simulation results for a calorimeter with two different samplings for the electromagnetic and hadronic compartments (see text). See Fig. 27 for the labelling.

Fig. 29 Measured neutron yield vs proton energy for various targets.

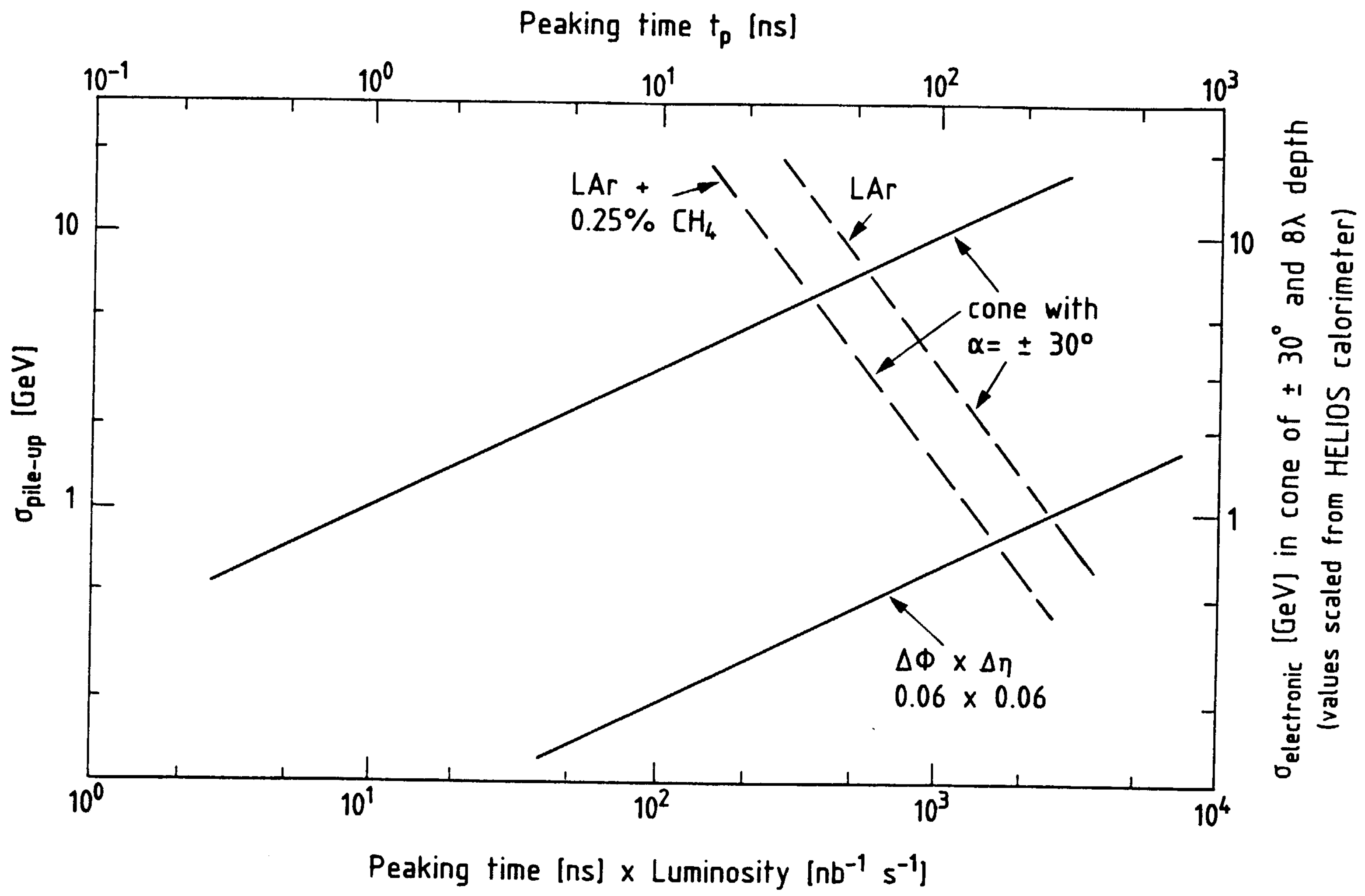
Peaking time t_p [ns]
10^{-1}
10^0
10^1
10^2
10^3
$\sigma_{pile-up}$ [GeV]
10
1
LAr +
0.25% CH_4
LAr
cone with
α= ± 30°
ΔΦ x Δη
0.06 x 0.06
$\sigma_{electronic}$ [GeV] in cone of ± 30° and 8λ depth
(values scaled from HELIOS calorimeter)
10^0
10^1
10^2
10^3
10^4
Peaking time [ns] x Luminosity [nb^{-1} s^{-1}]

Fig. 1

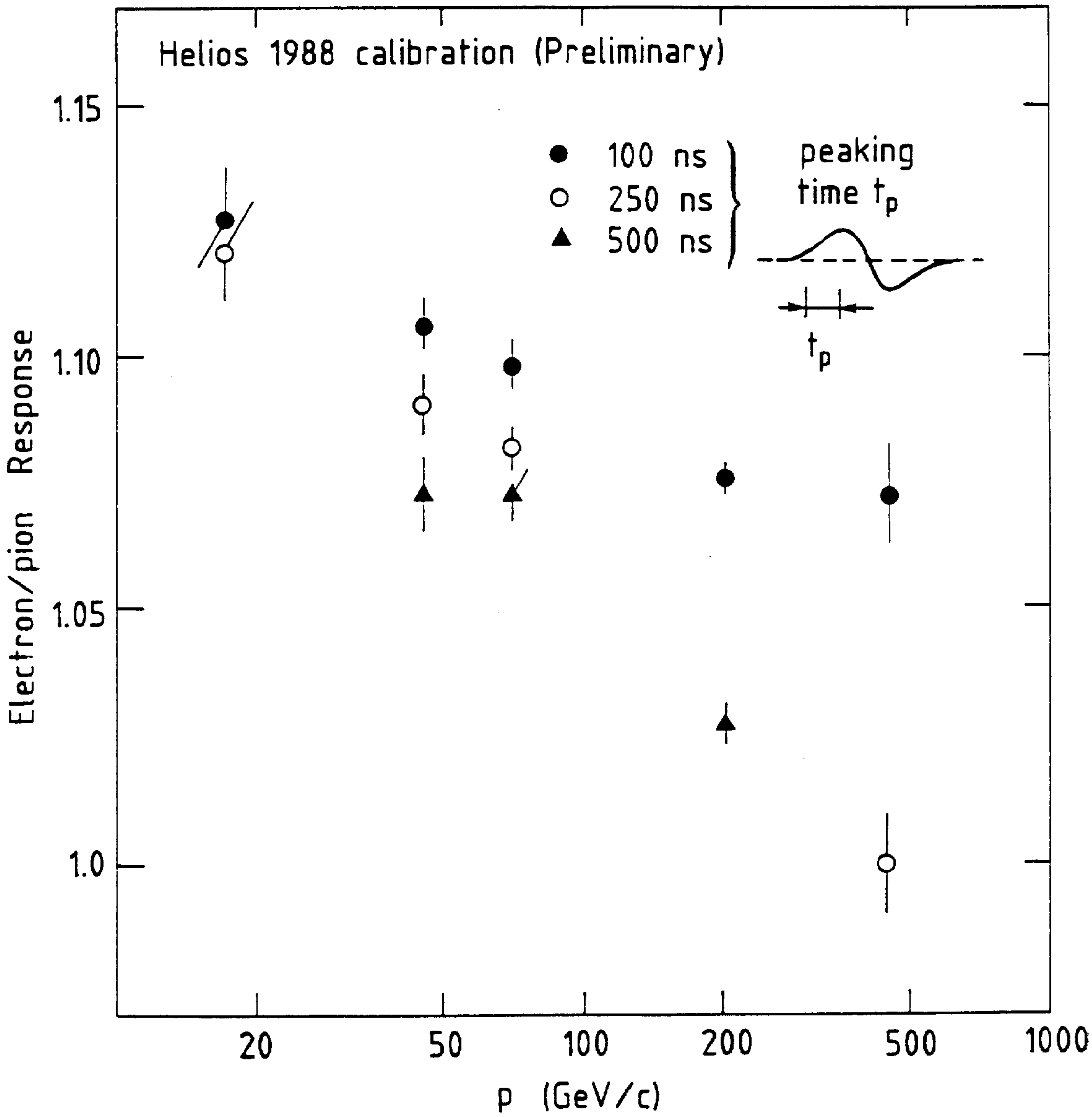

Helios 1988 calibration (Preliminary)
100 ns
250 ns
500 ns
peaking time t_p
t_p
1.15
1.10
1.05
1.0
Electron/pion Response
20
50
100
200
500
1000
p (GeV/c)

Fig. 2

a)

b)

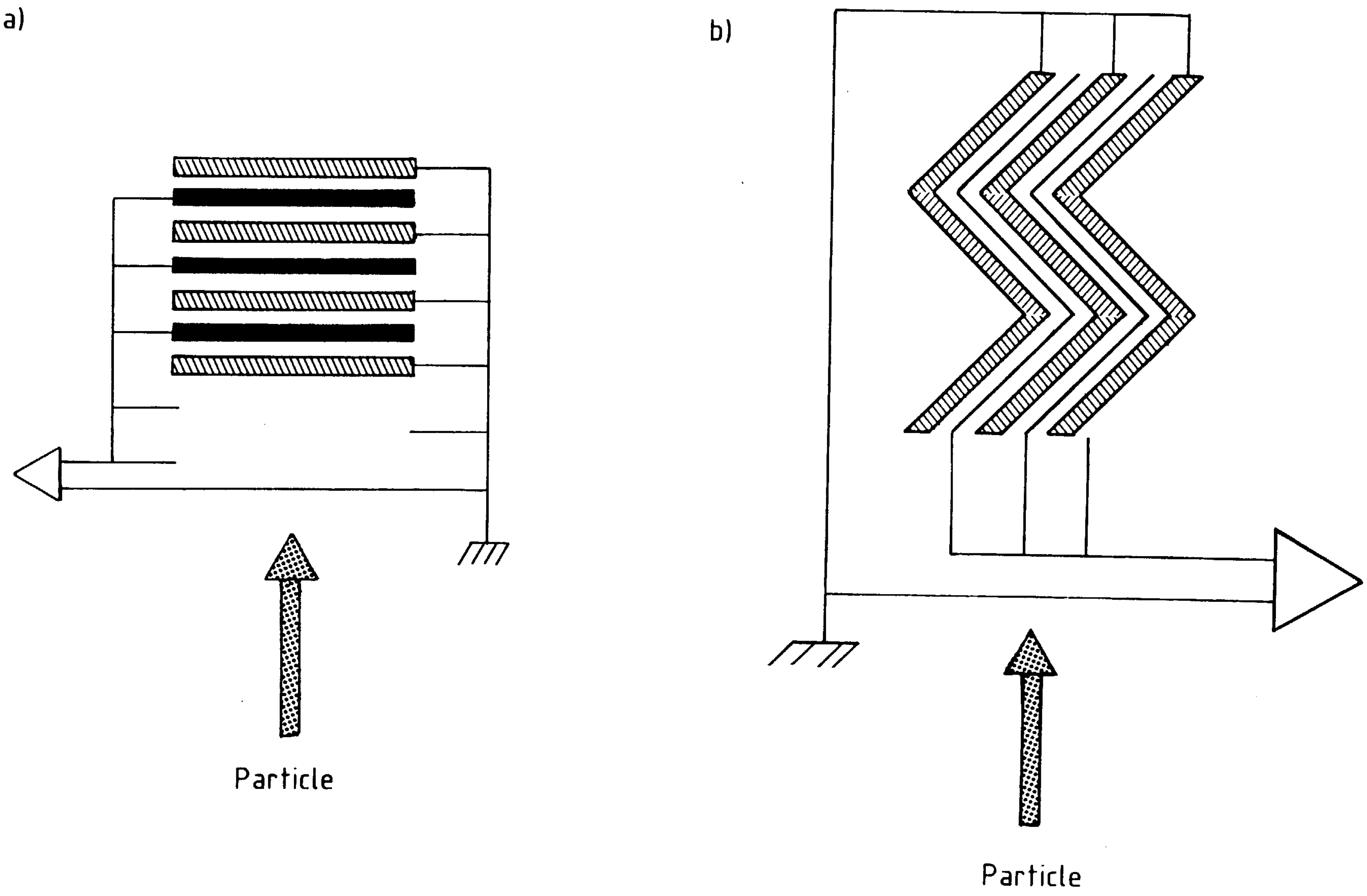

Fig. 3

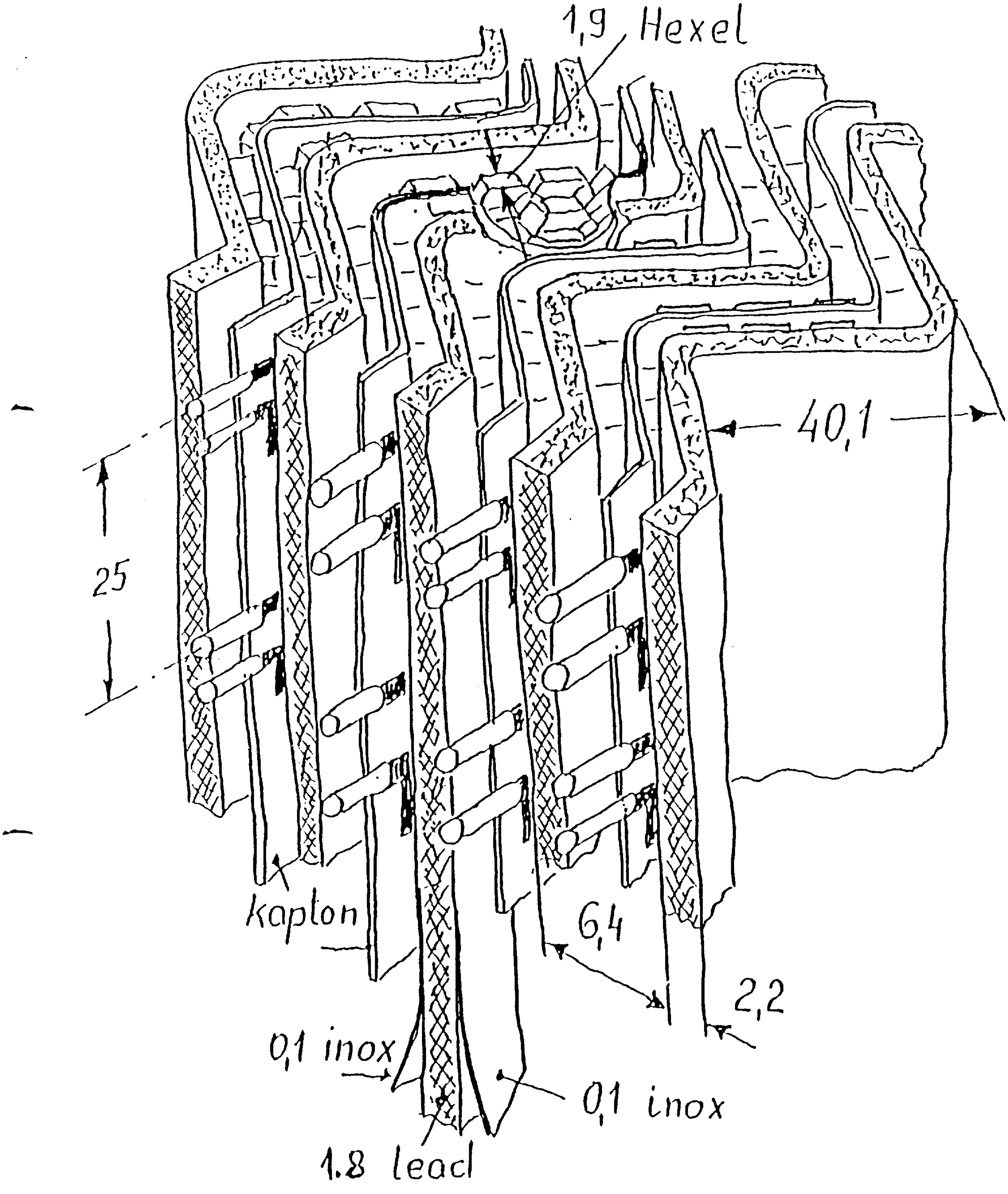

Fig. 4

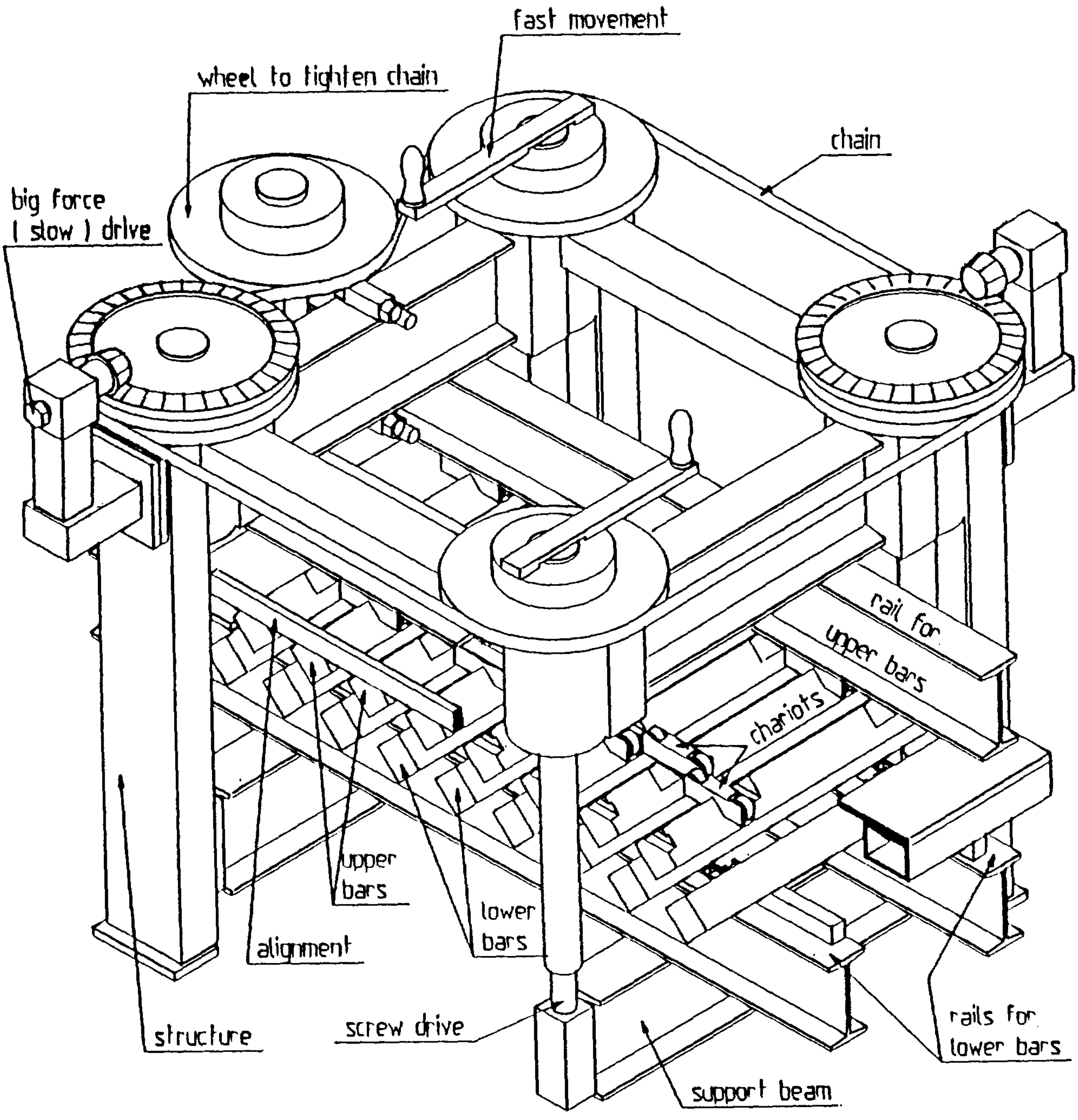
fast movement
wheel to tighten chain
chain
big force
(slow) drive
rail for
upper bars
chariots
upper
bars
lower
bars
alignment
structure
screw drive
rails for
lower bars
support beam

Fig.5

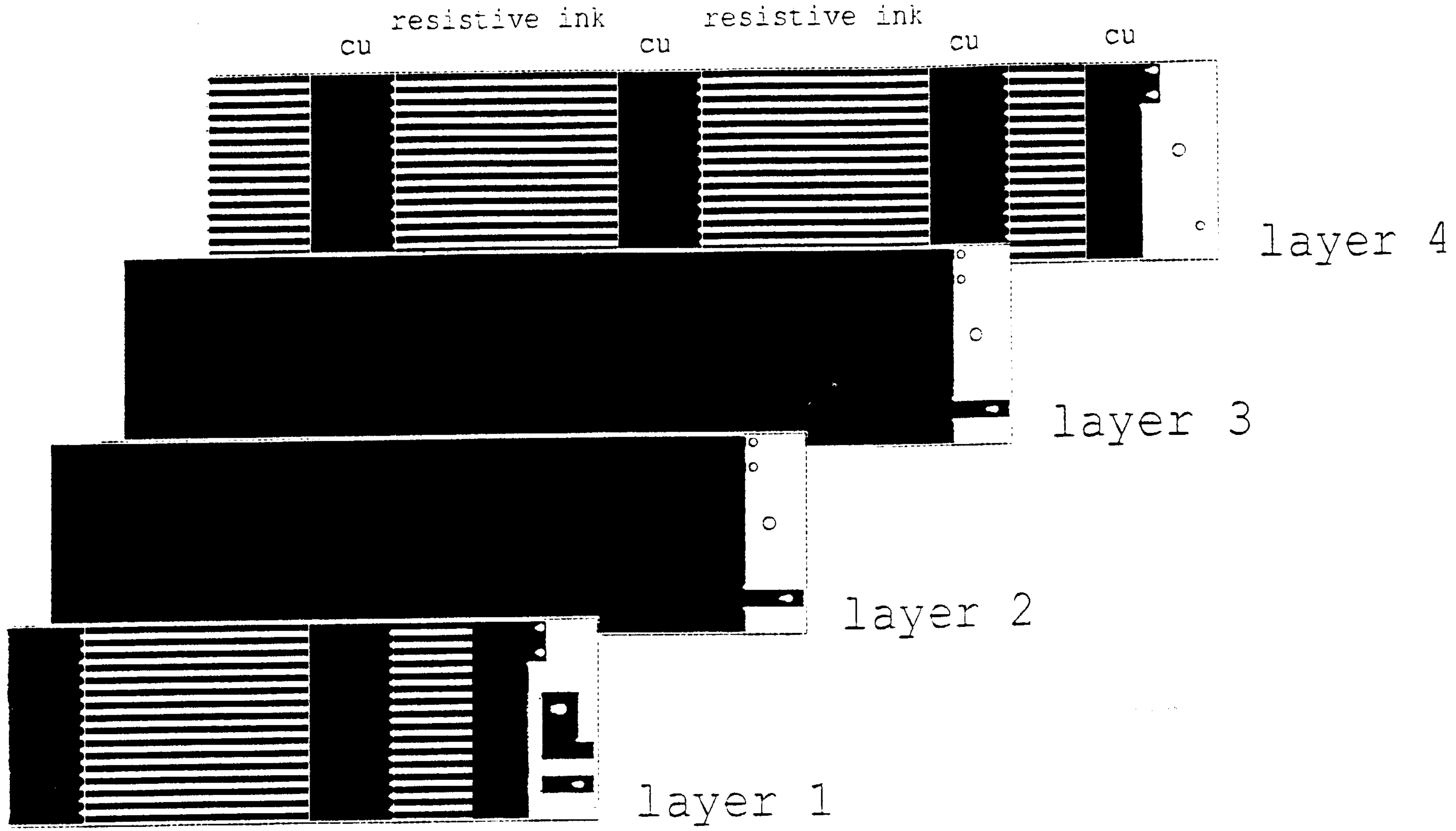

resistive ink
resistive ink
cu
cu
cu
cu
layer 4
layer 3
layer 2
layer 1

Fig. 6

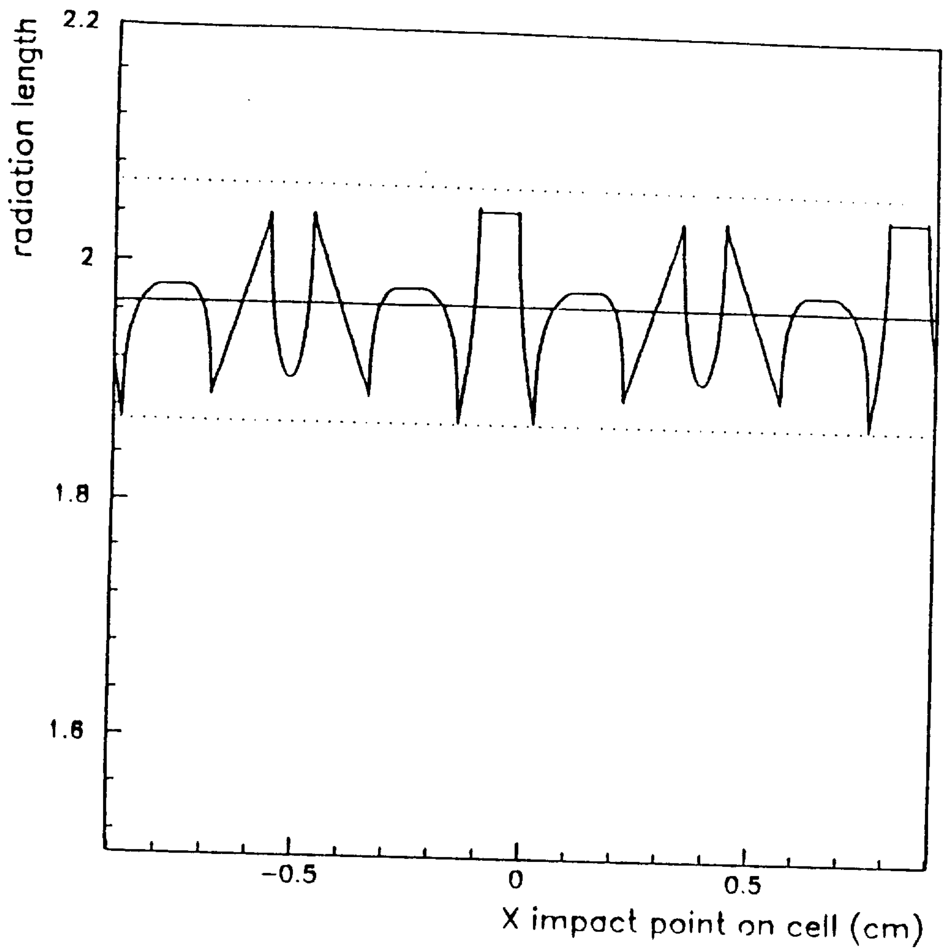

Fig. 7

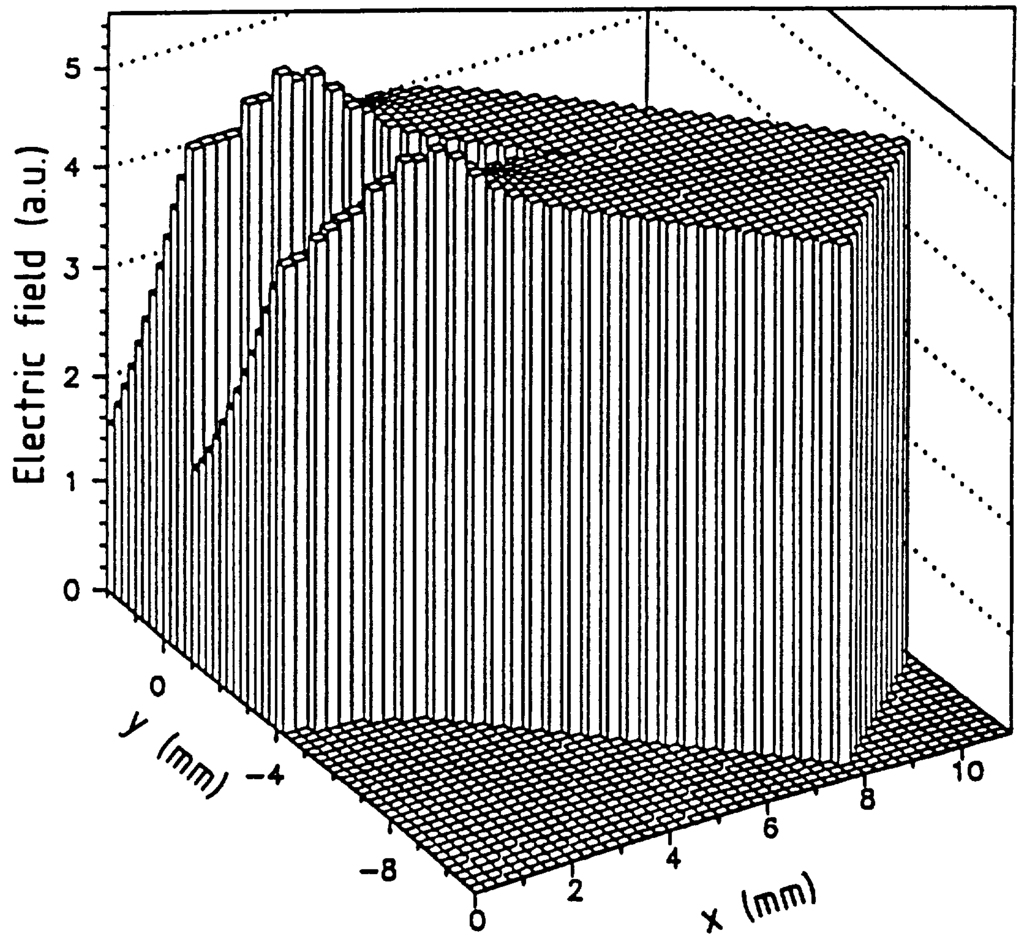

Fig. 8

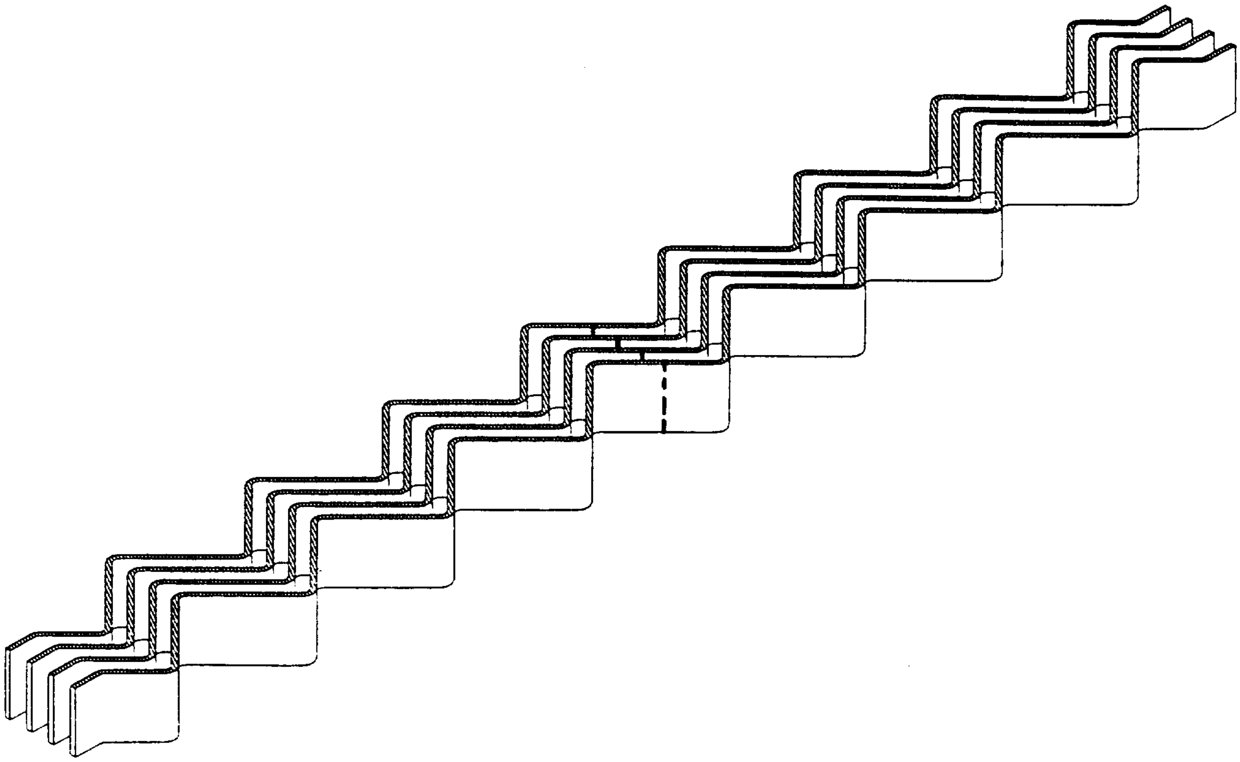

Fig. 9

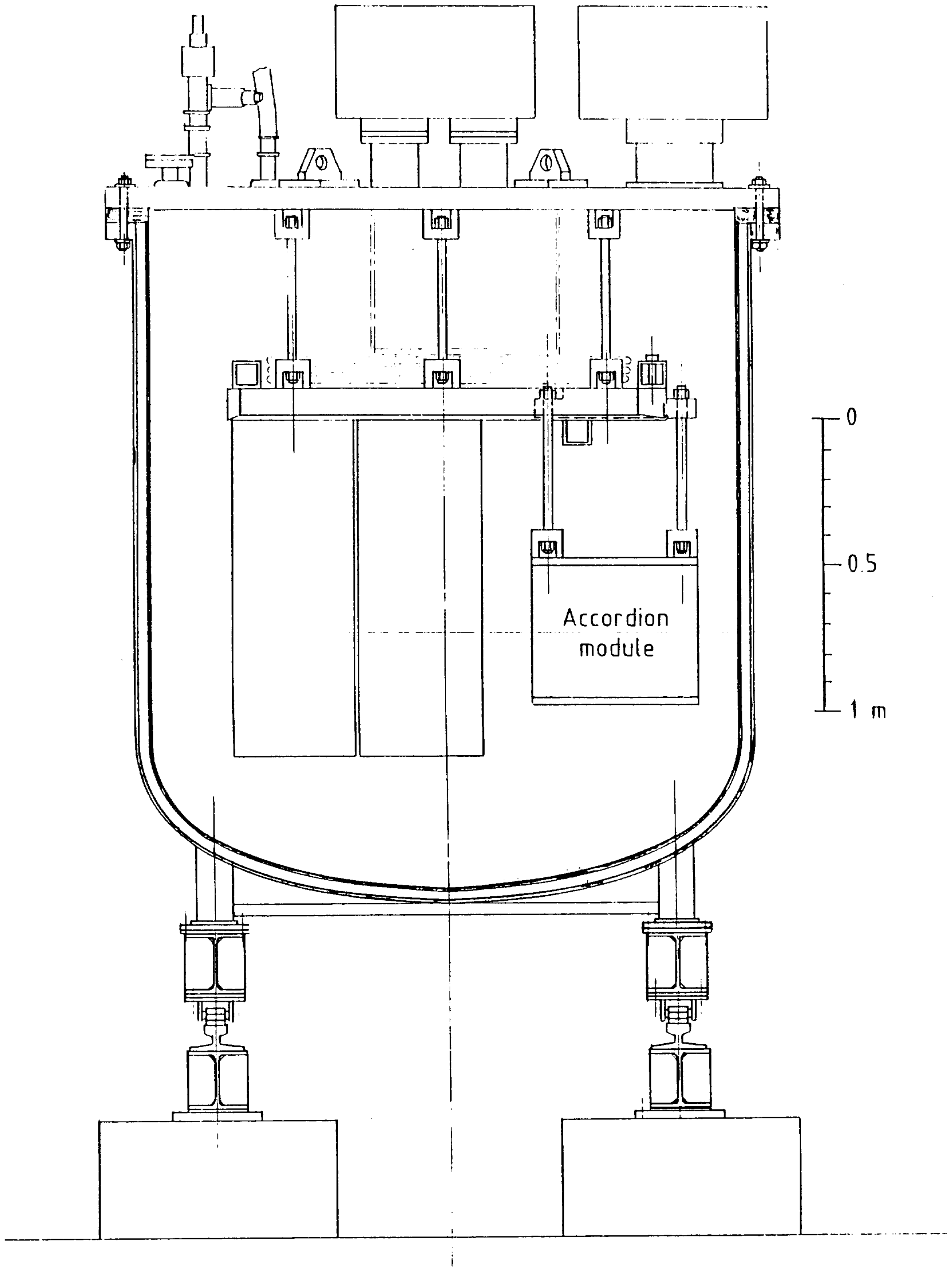

Fig. 12

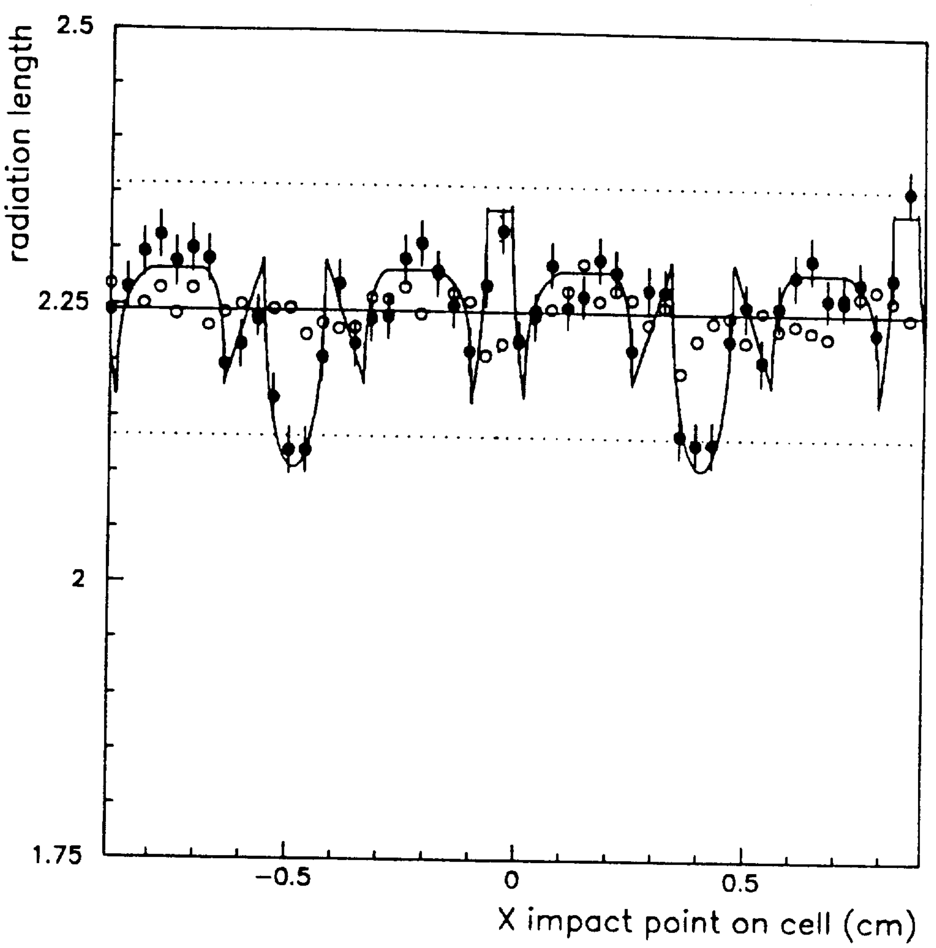

Fig. 13

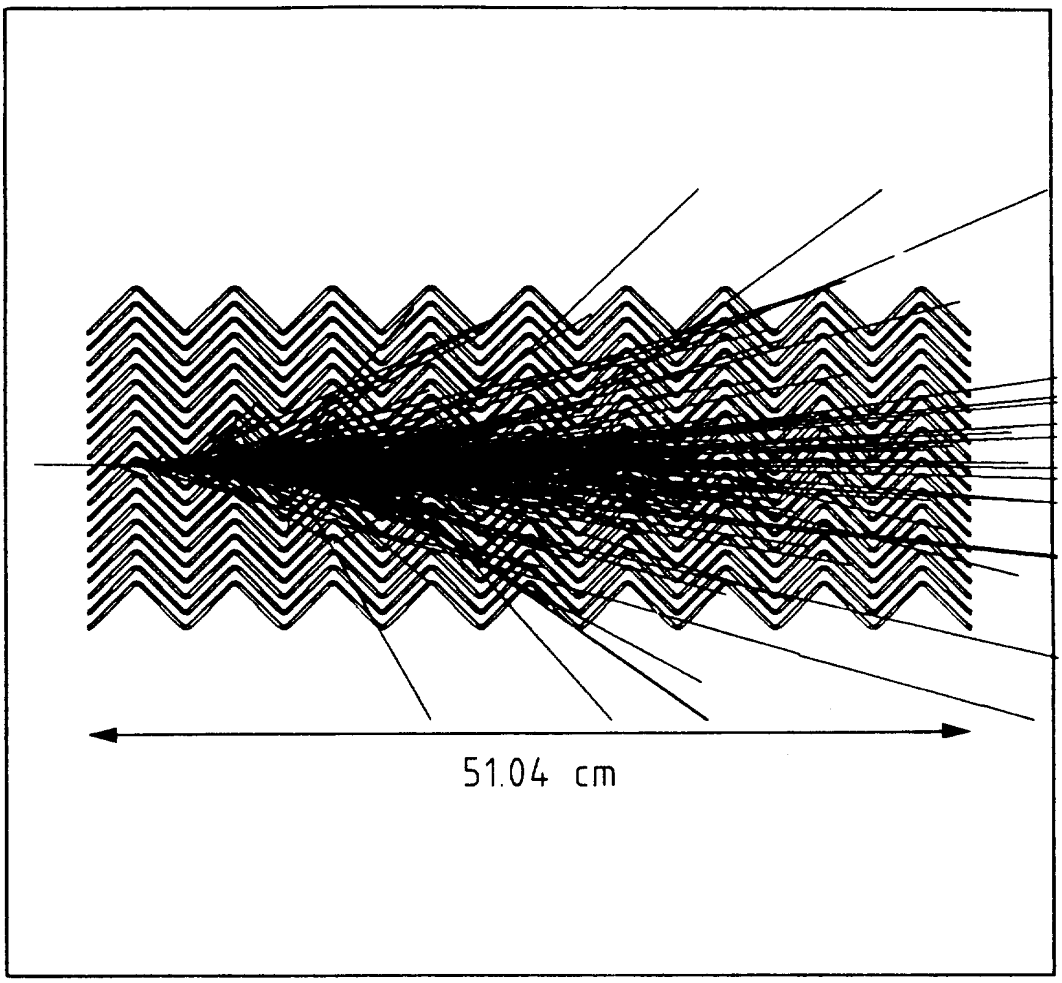

Fig. 14 a

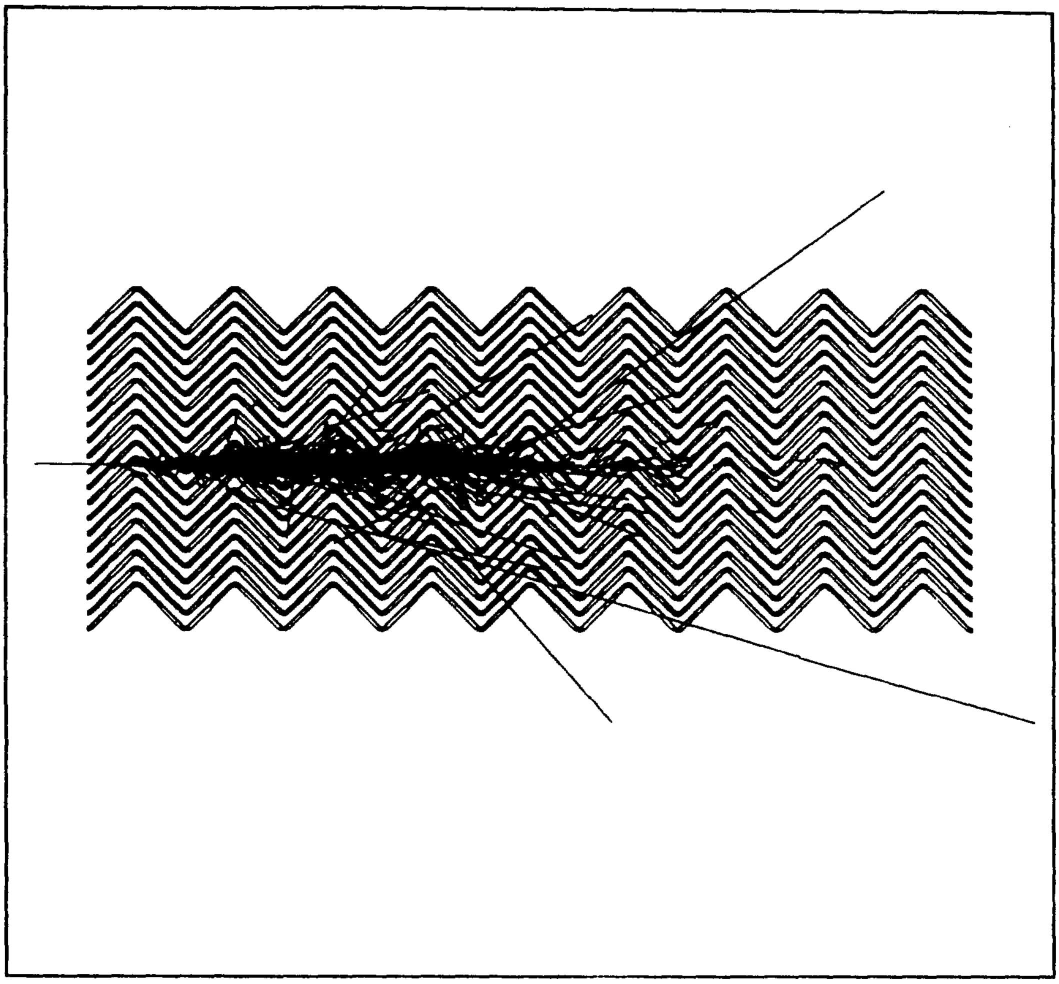

Fig. 14 b

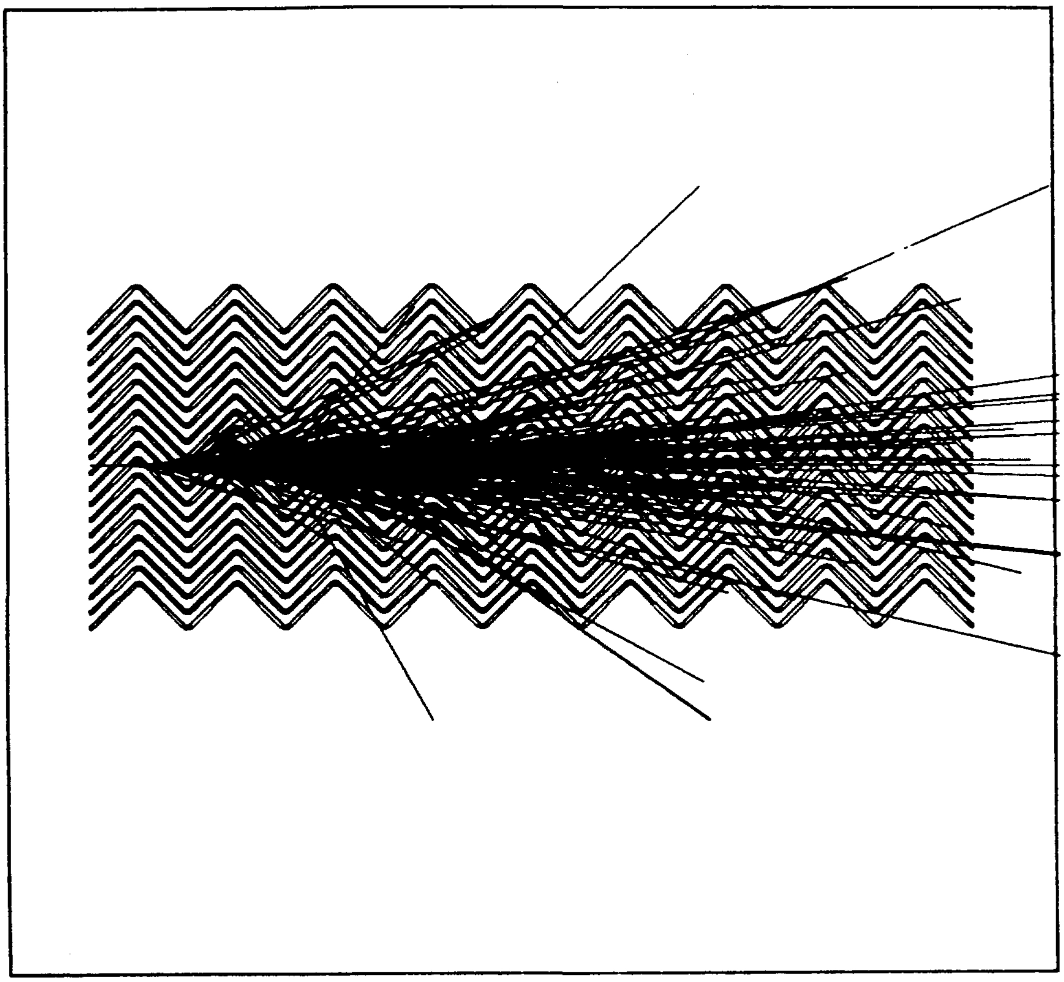

Fig. 14 c

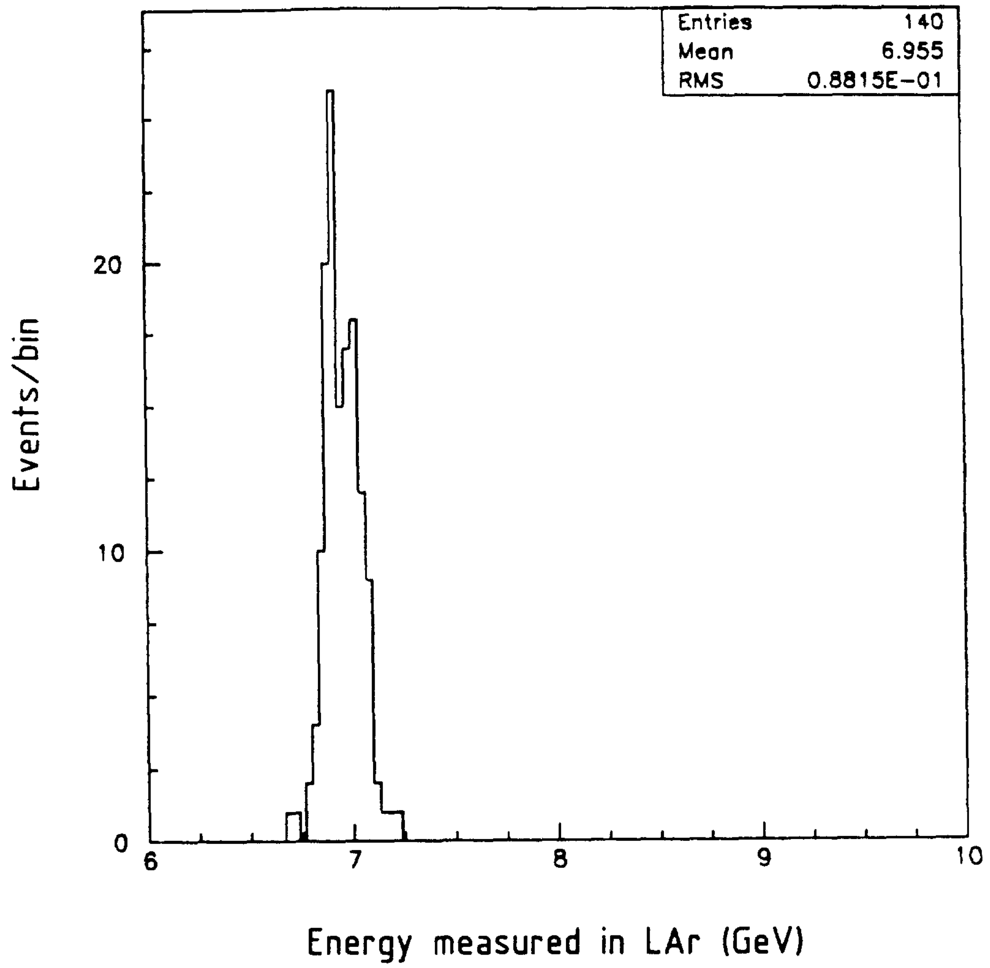

Entries 140
Mean 6.955
RMS 0.8815E-01
Events/bin
0
10
20
6
7
8
9
10
Energy measured in LAr (GeV)

Fig. 15

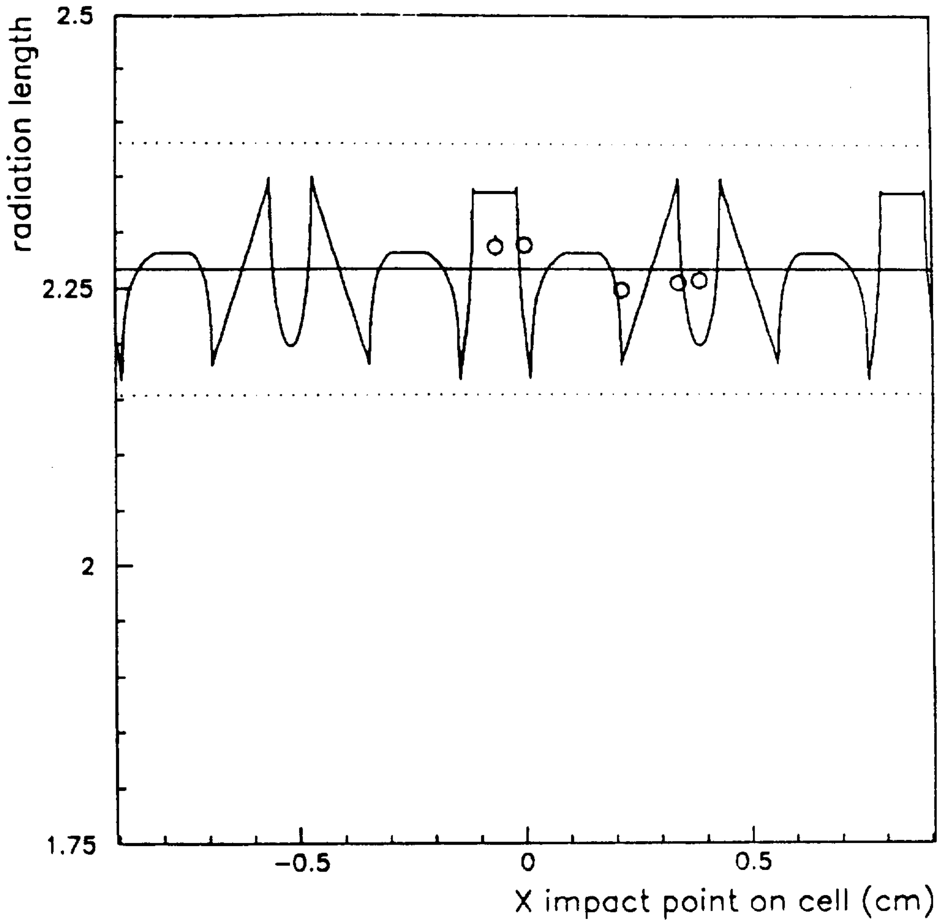

Fig. 16

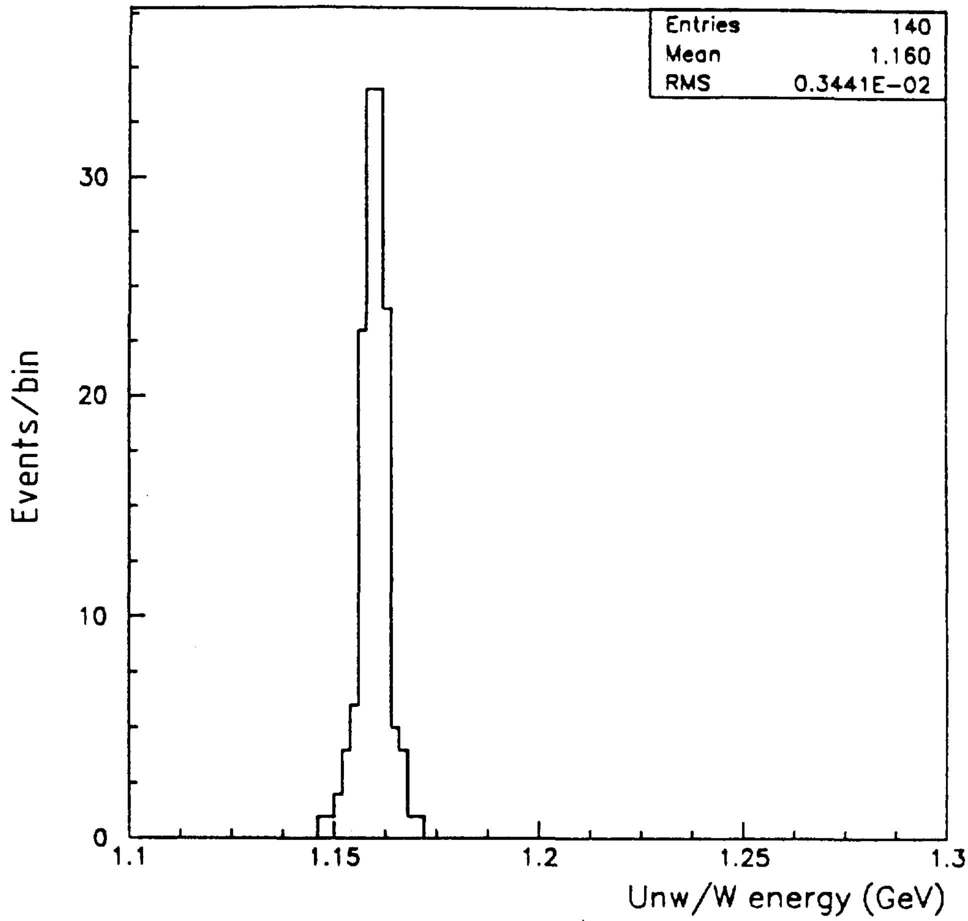

Deposited/collected energy

Fig. 17

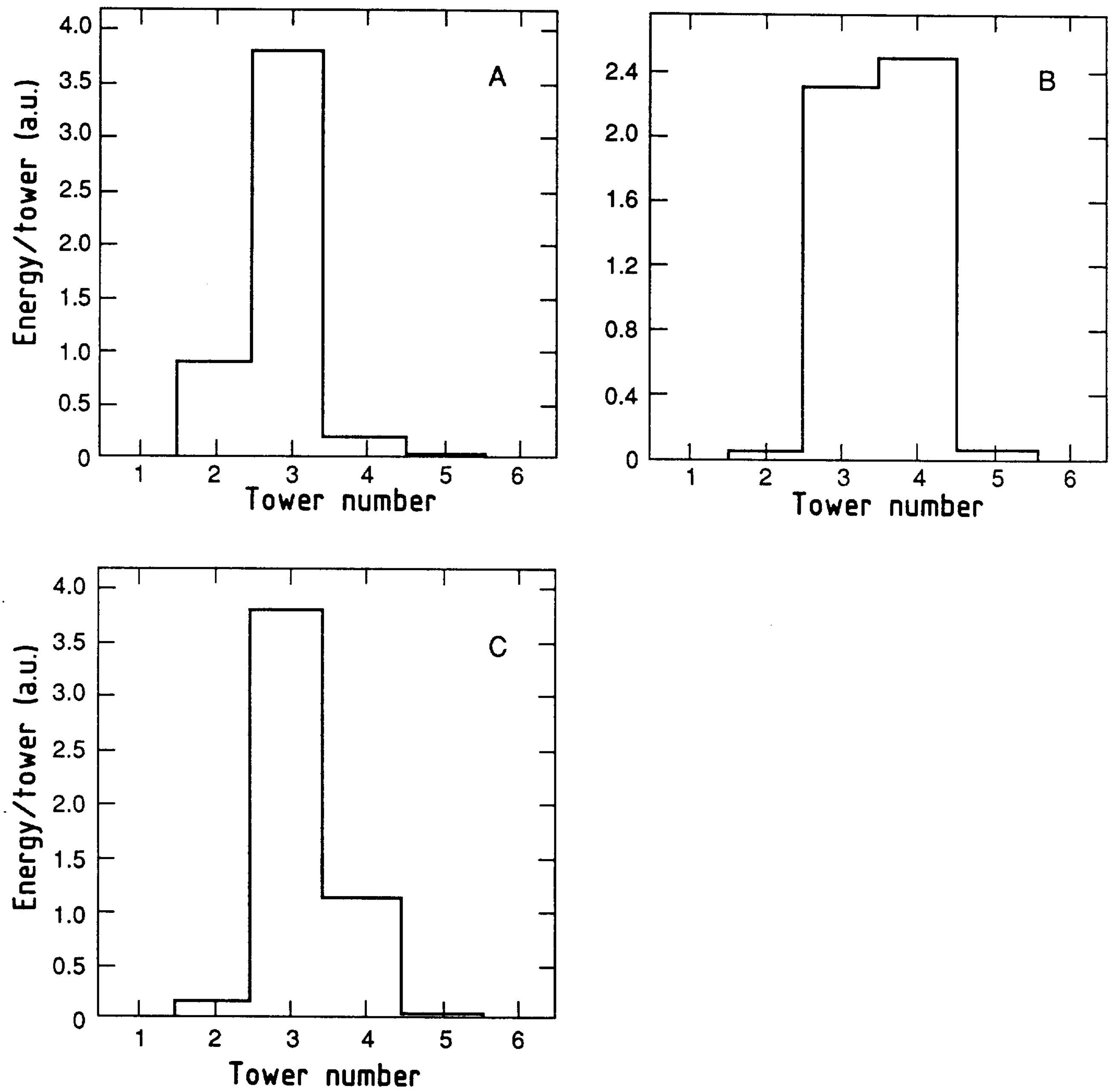
A
B
C
Energy/tower (a.u.)
Tower number
4.0
3.5
3.0
2.5
2.0
1.5
1.0
0.5
0
2.4
2.0
1.6
1.2
0.8
0.4
1
2
3
4
5
6

Fig. 18

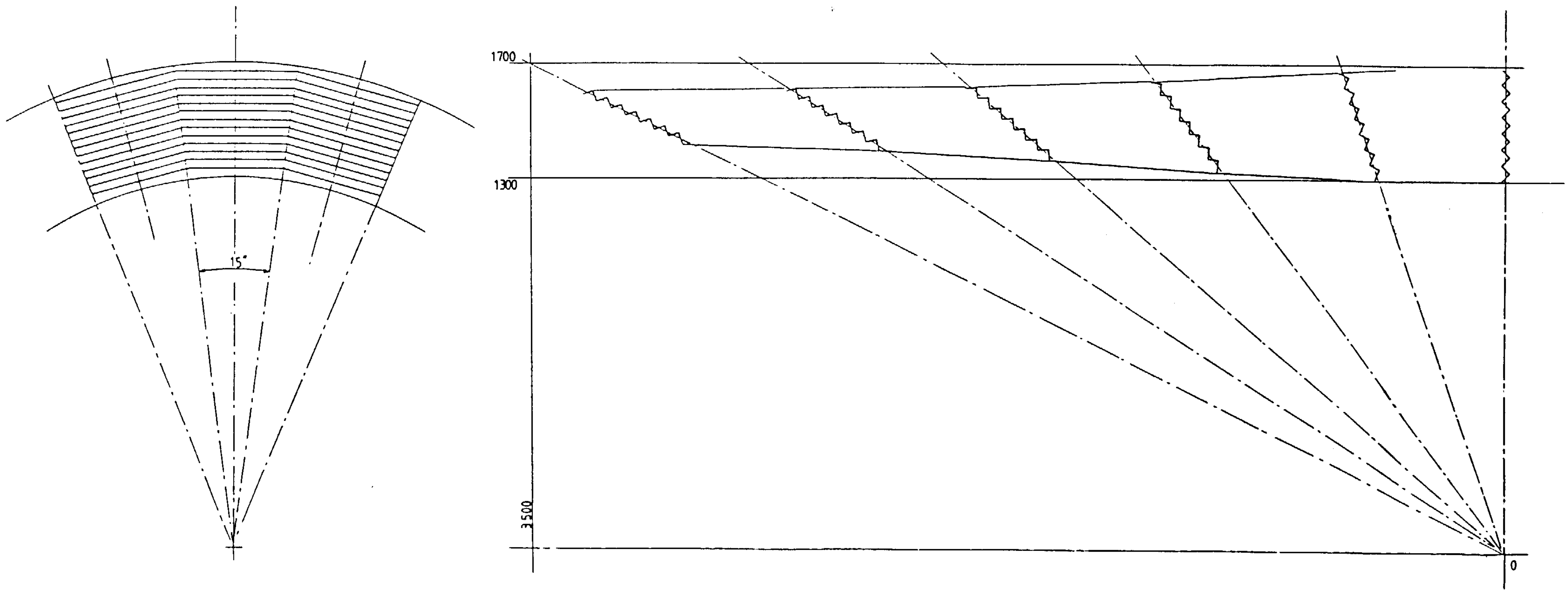

Fig. 19 a

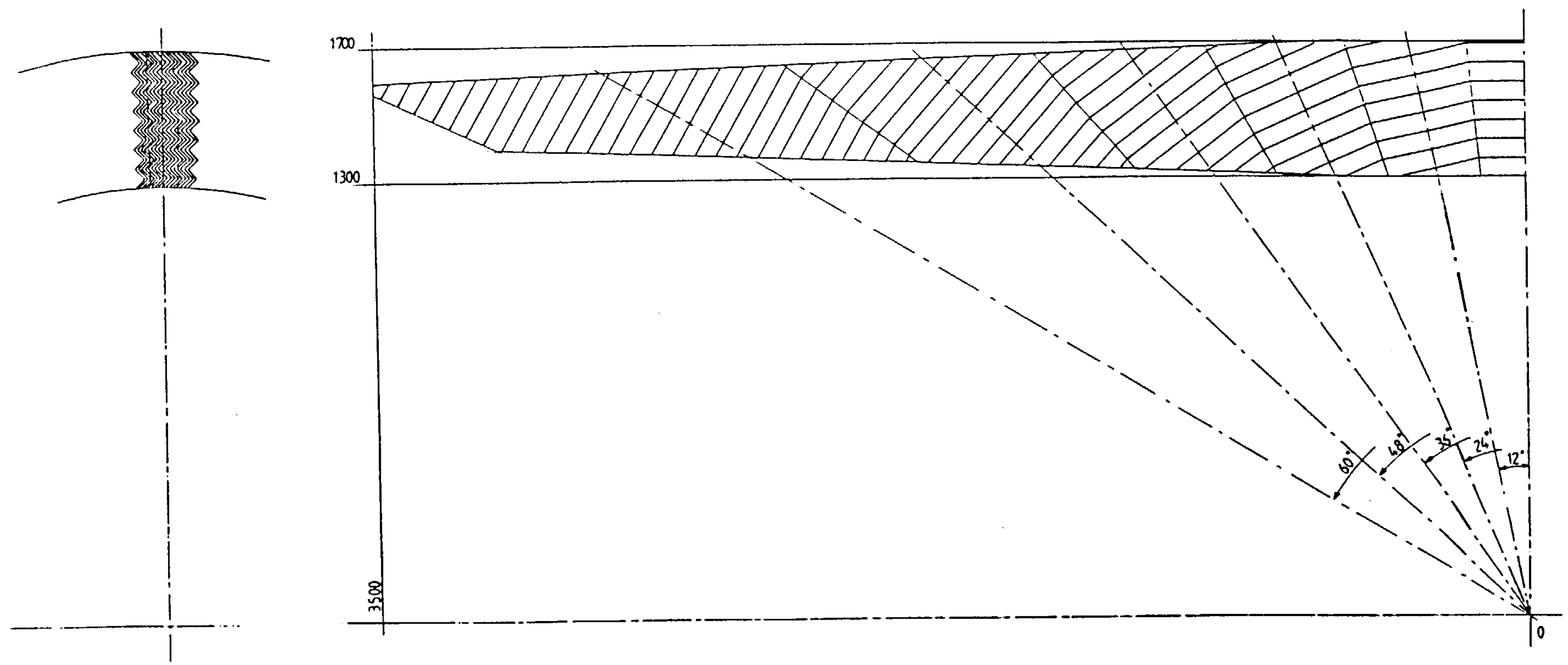

Fig. 19 b

a) Parallel connection **b) Series connection**

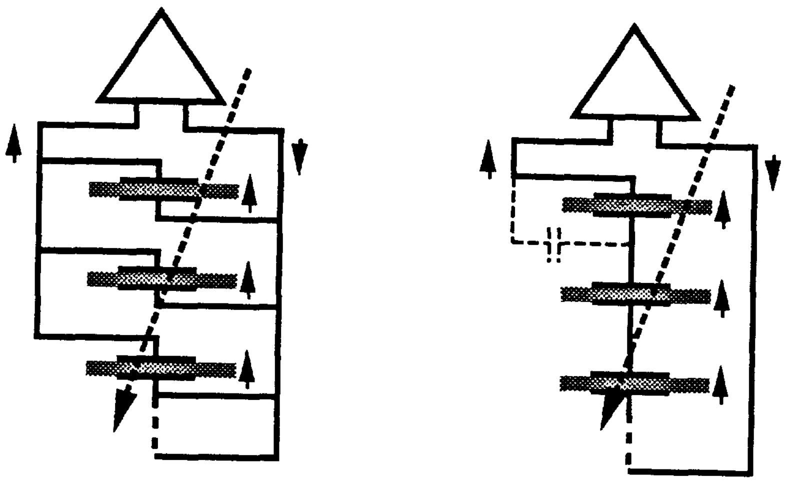

a)

$C_{tot} = p \times C_{gap}$

$I_{tot} = p \times I_{gap}$

Signal / Noise $\approx \sqrt{p}$

b)

$C_{tot} = C_{gap} / s$

$I_{tot} = \langle I_{gap} \rangle$

Signal / Noise $\approx \sqrt{s}$

Fig. 20

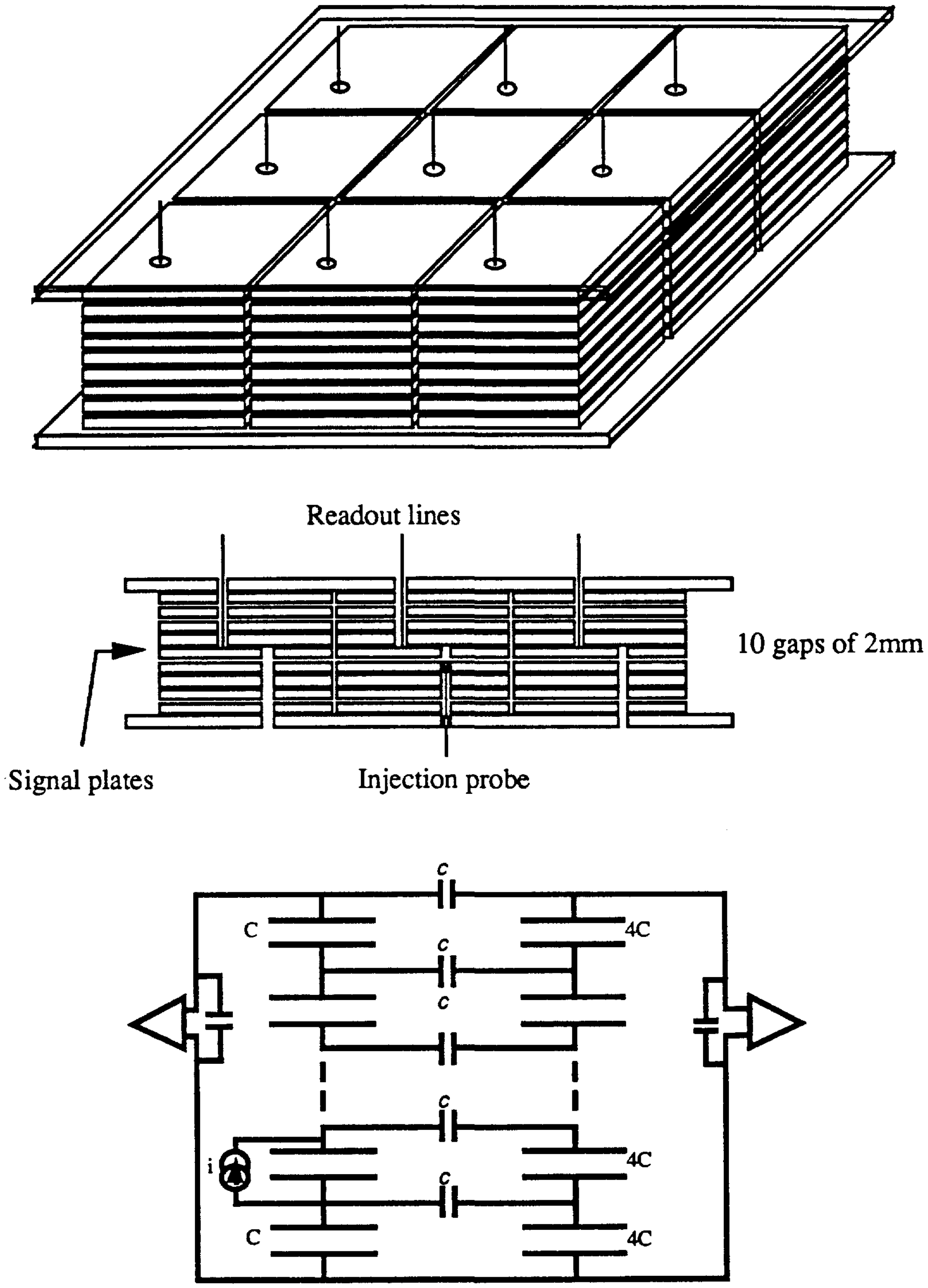
Readout lines
10 gaps of 2mm
Signal plates
Injection probe
c
C
4C
i

Fig. 21

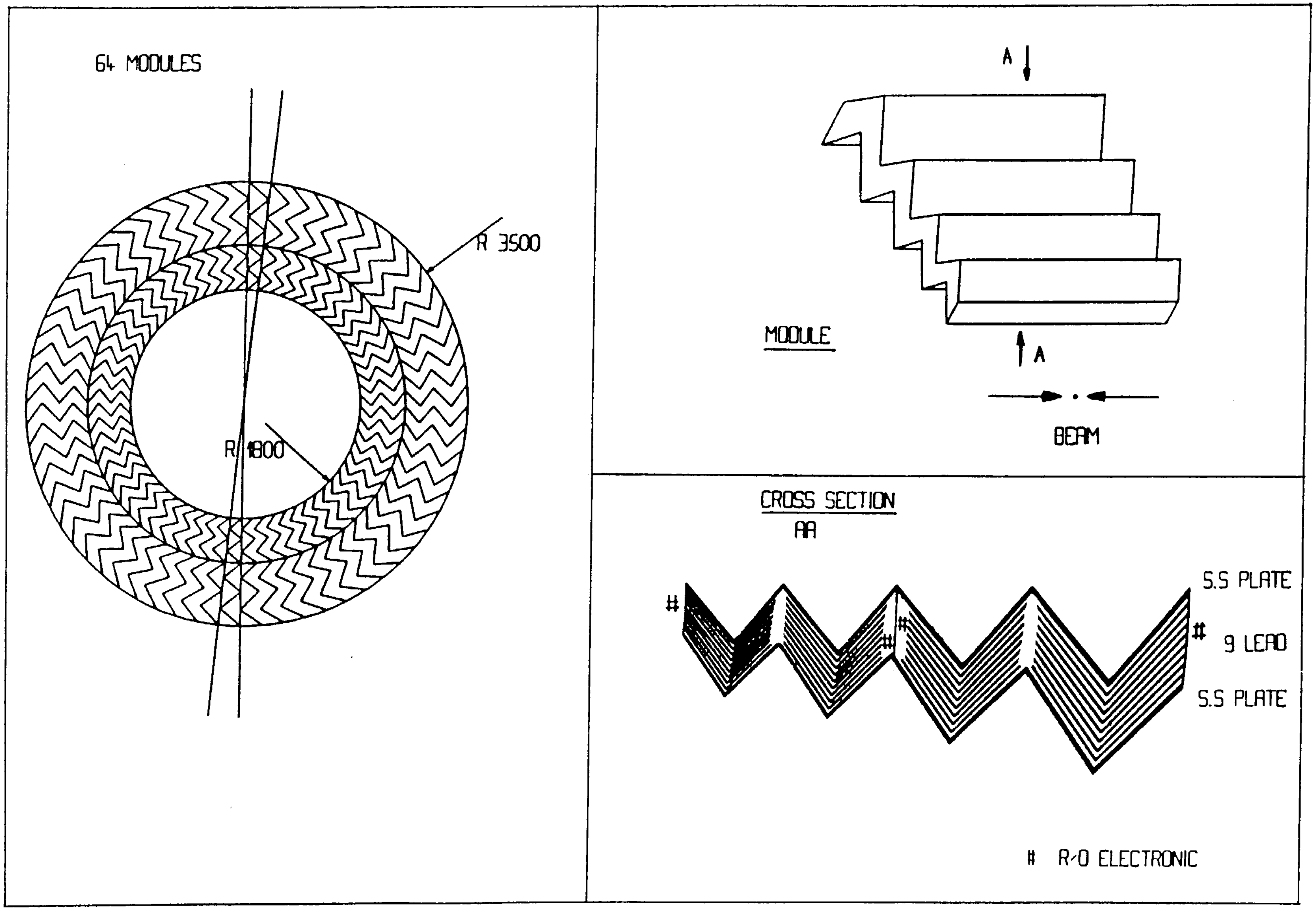
64 MODULES
R 3500
R 1800
A
MODULE
A
BEAM
CROSS SECTION
AA
S.S PLATE
9 LEAD
S.S PLATE
#
R/O ELECTRONIC

Fig. 22

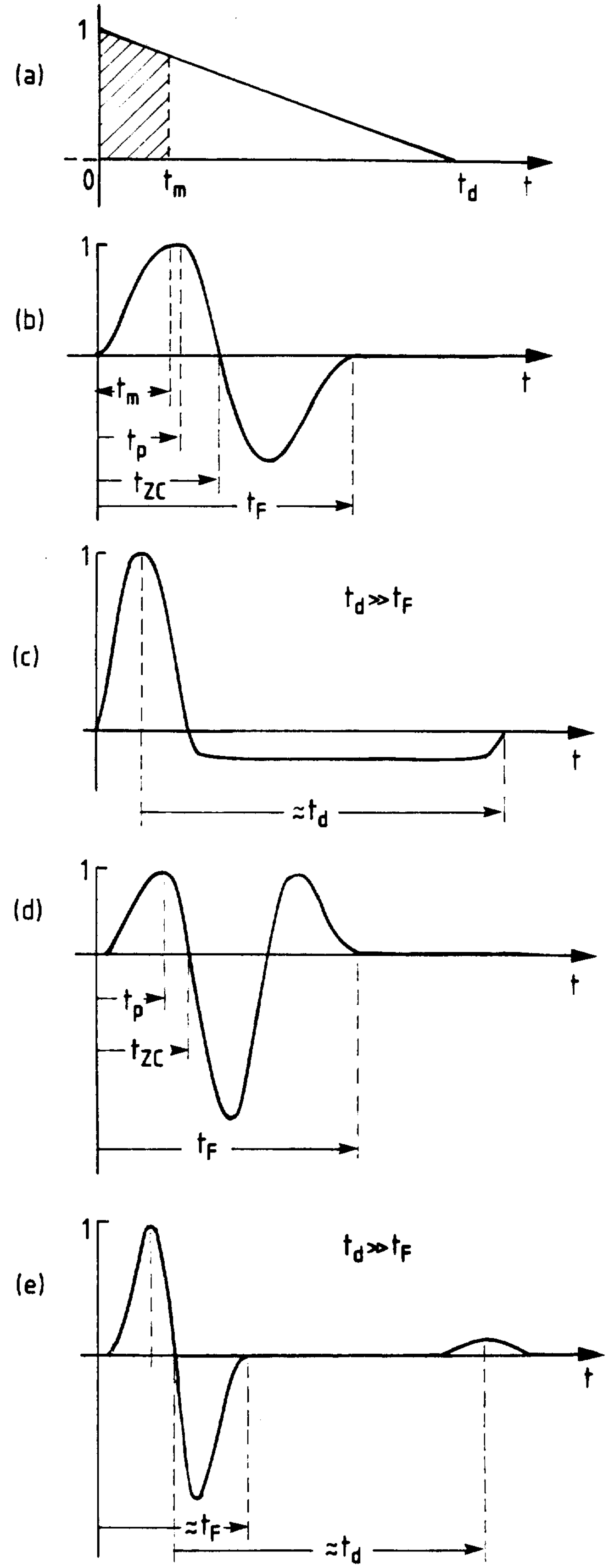
(a)
1
0
t_m
t_d
t
(b)
1
t_m
t_p
t_{ZC}
t_F
t
(c)
1
$t_d \gg t_F$
$\approx t_d$
t
(d)
1
t_p
t_{ZC}
t_F
t
(e)
1
$t_d \gg t_F$
$\approx t_F$
$\approx t_d$
t

Fig. 23

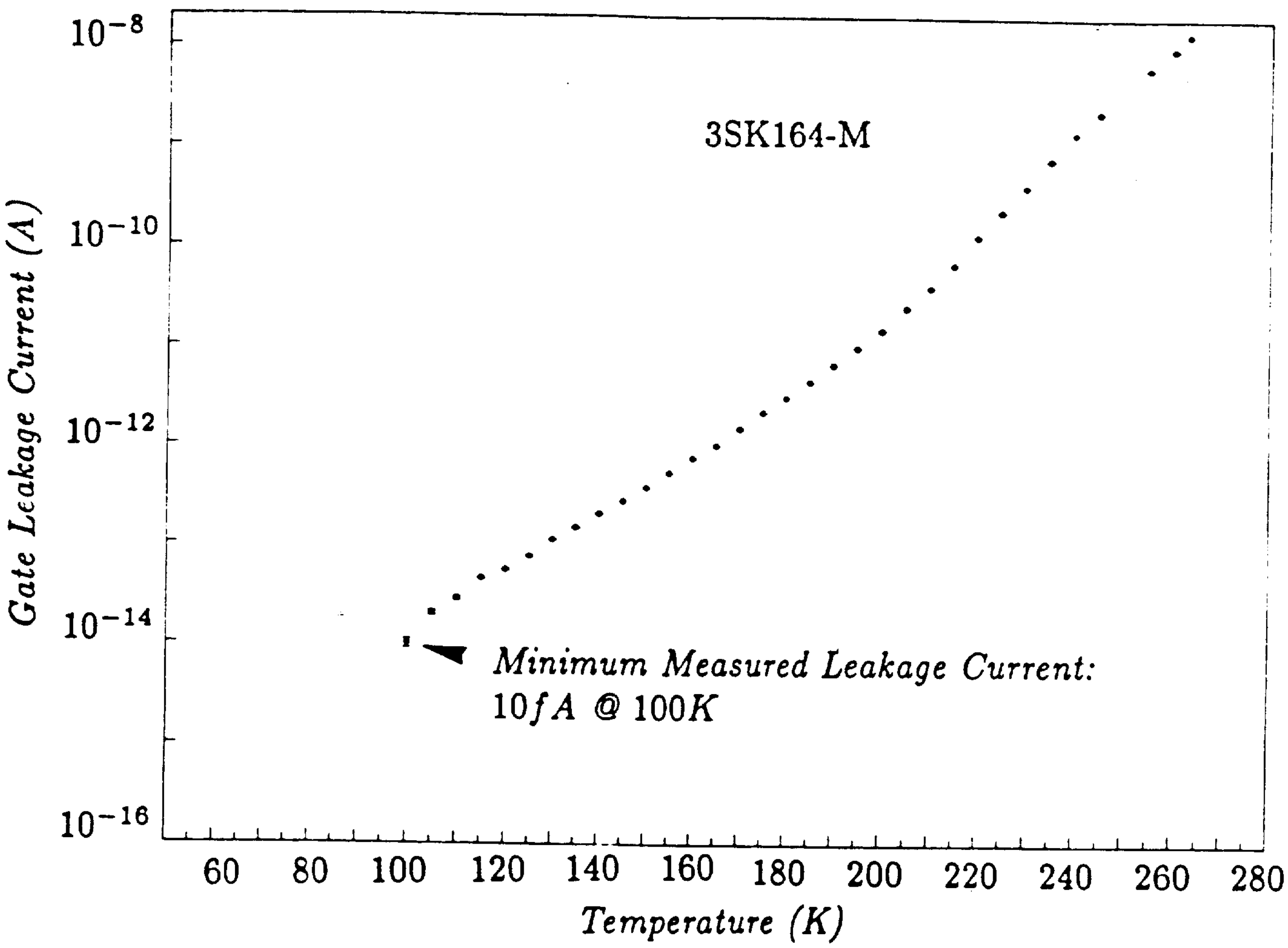
3SK164-M
Gate Leakage Current (A)
10^{-8}
10^{-10}
10^{-12}
10^{-14}
10^{-16}
Minimum Measured Leakage Current:
10fA @ 100K
60 80 100 120 140 160 180 200 220 240 260 280
Temperature (K)

Fig. 24

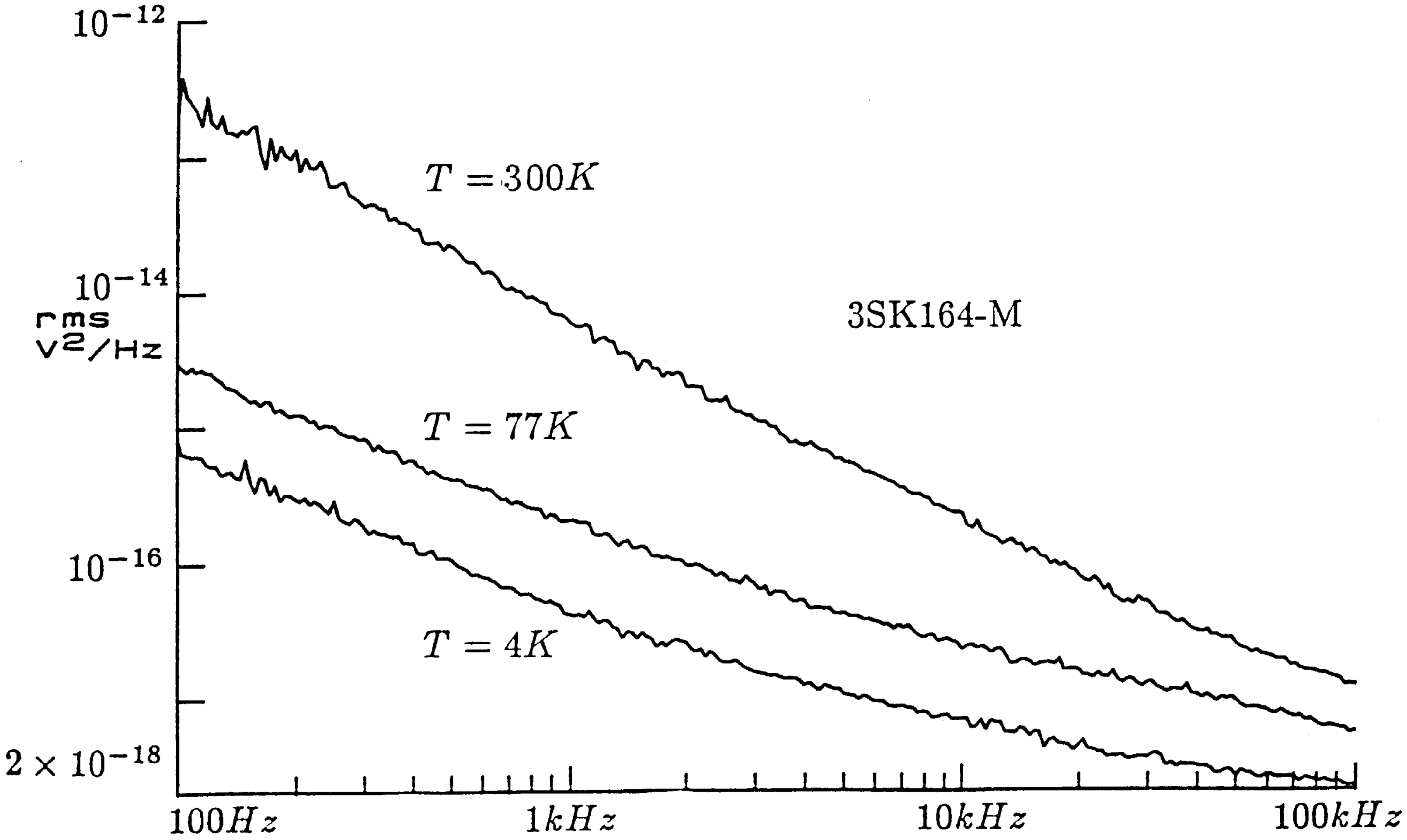

10−12
10−14
rms V2/Hz
10−16
2 × 10−18
T = 300K
T = 77K
T = 4K
3SK164-M
100Hz
1kHz
10kHz
100kHz

Fig. 25

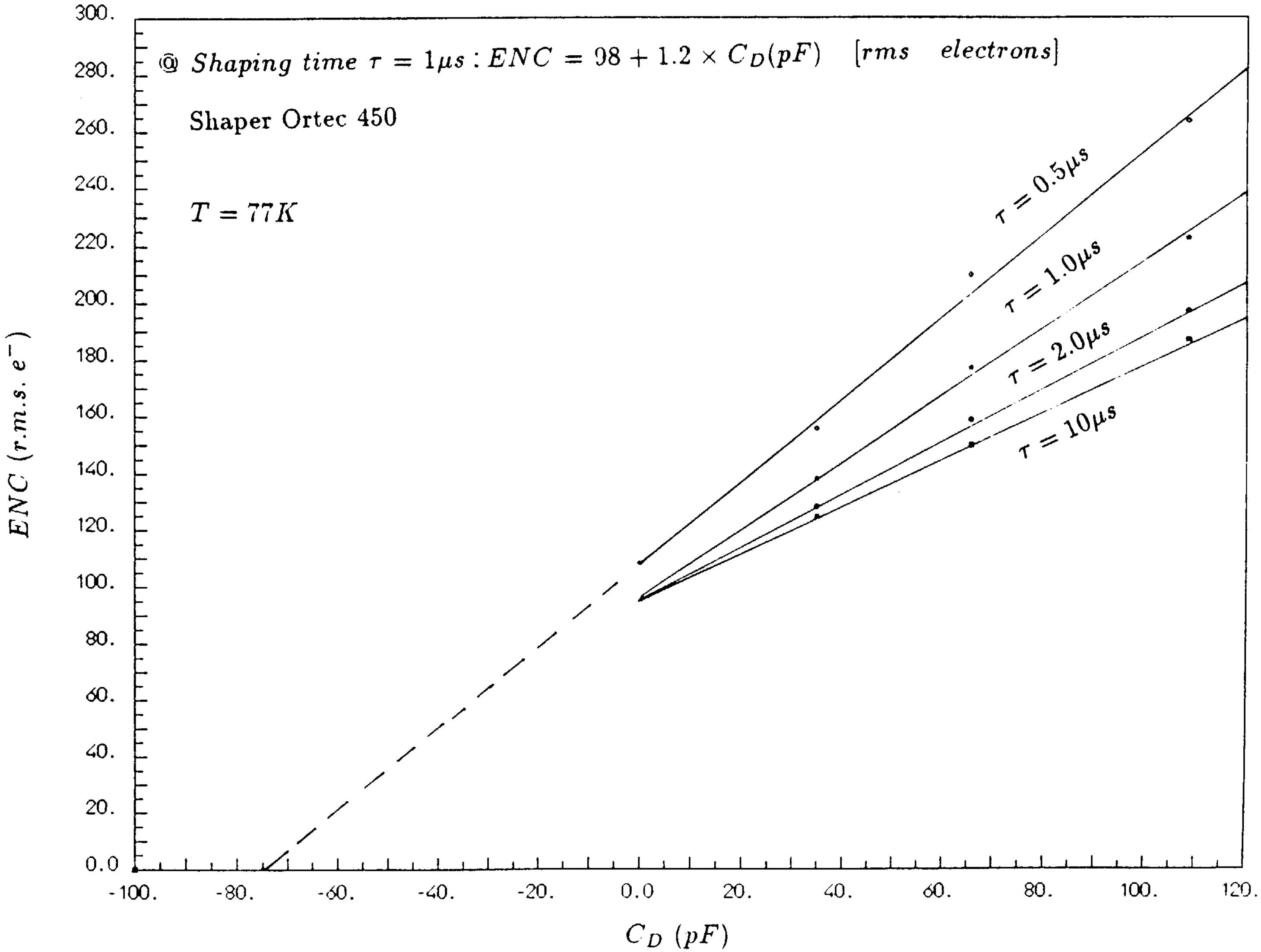
@ Shaping time $\tau = 1\mu s : ENC = 98 + 1.2 \times C_D(pF)$ [rms electrons]
Shaper Ortec 450
$T = 77K$
$\tau = 0.5\mu s$
$\tau = 1.0\mu s$
$\tau = 2.0\mu s$
$\tau = 10\mu s$
ENC ($r.m.s.$ e^-)
300.
280.
260.
240.
220.
200.
180.
160.
140.
120.
100.
80.
60.
40.
20.
0.0
-100.
-80.
-60.
-40.
-20.
0.0
20.
40.
60.
80.
100.
120.
C_D (pF)

Fig. 26

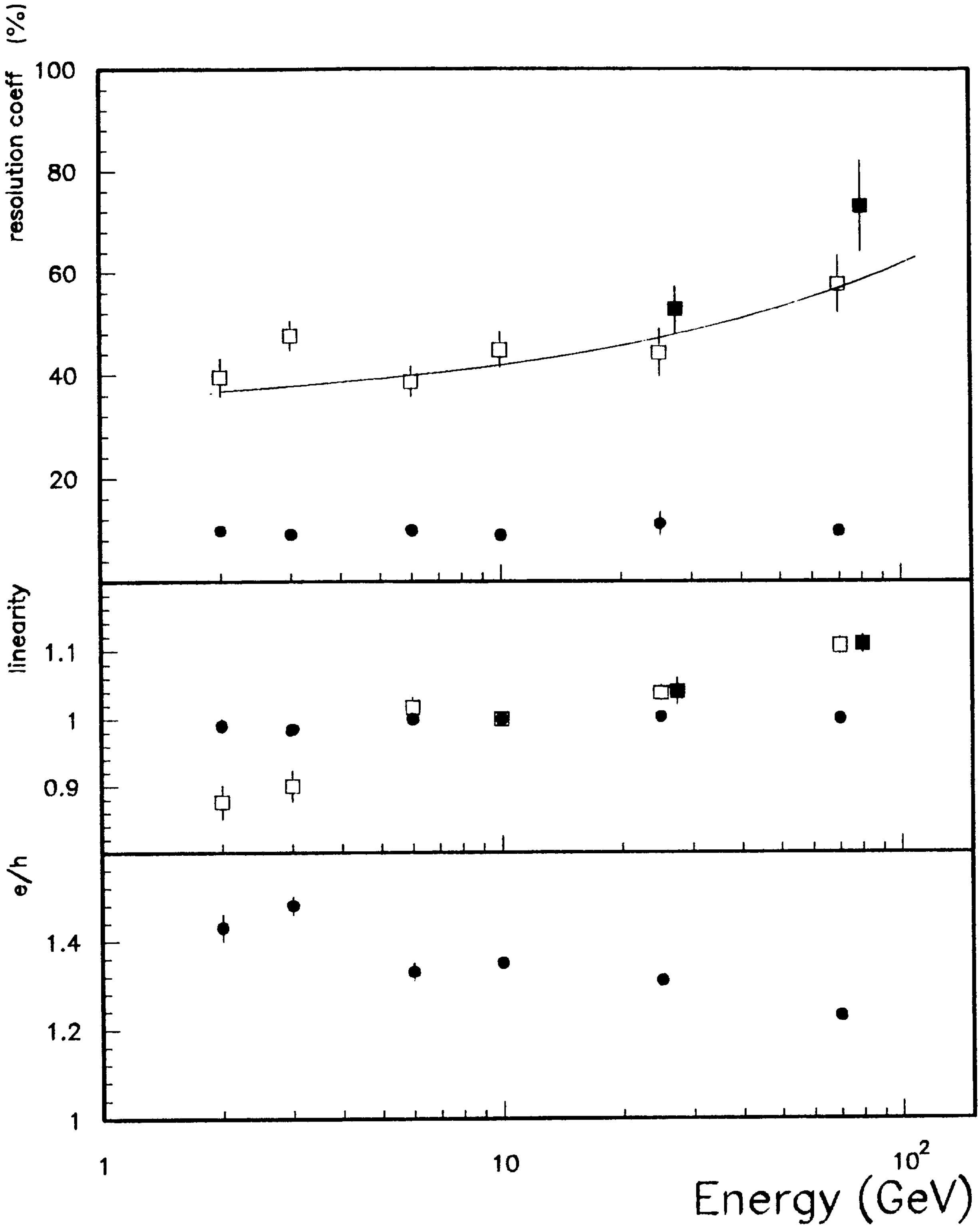

resolution coeff (%)
100
80
60
40
20
linearity
1.1
1
0.9
e/h
1.4
1.2
1
1
10
10^2
Energy (GeV)

Fig. 27

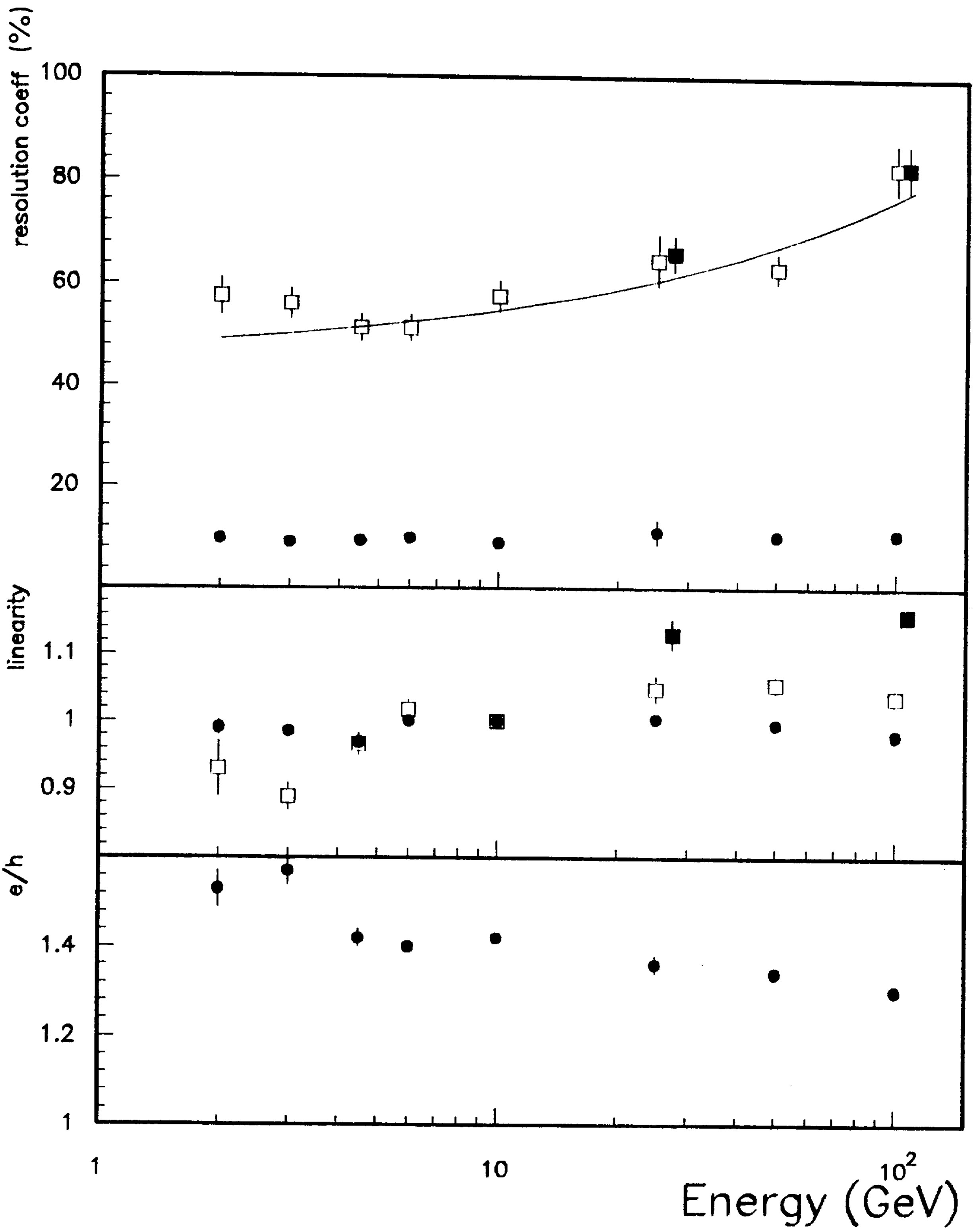

resolution coeff (%)
100
80
60
40
20
linearity
1.1
1
0.9
e/h
1.4
1.2
1
1
10
10^2
Energy (GeV)

Fig. 28

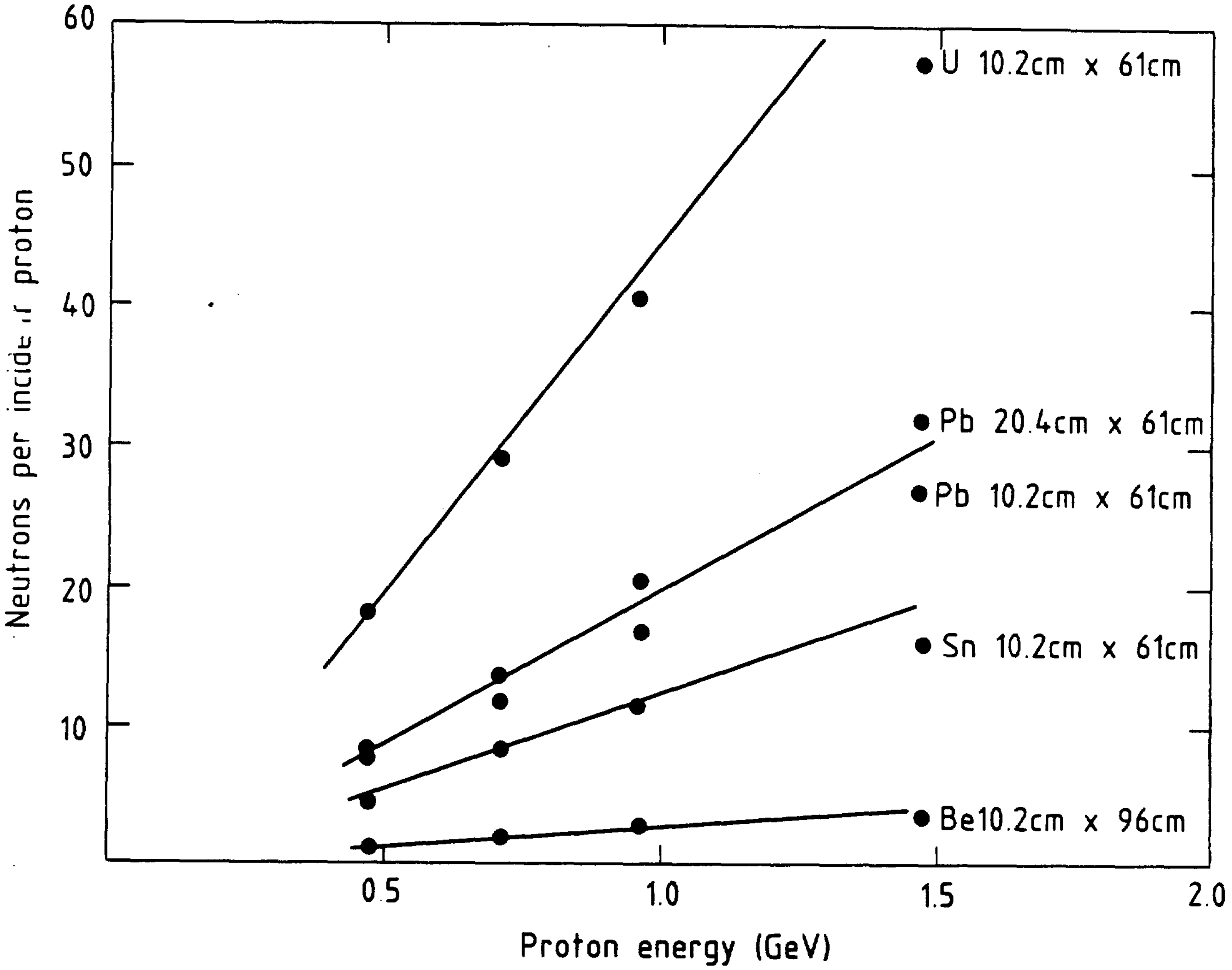

Fig. 29

Imprimé au CERN. Prix : 2.90 Fr.